Coupling halide perovskites with different materials: From doping to nanocomposites, beyond photovoltaics

Coupling halide perovskites with different materials: from doping to nanocomposites, beyond photovoltaics

Marcello Righetto,[1] Daniele Meggiolaro,[2,3] Antonio Rizzo,[4,5] Roberto Sorrentino,[6] Gaudenzio Meneghesso,[4,5] Tze Chien Sum,[1*] Teresa Gatti,[7*] Francesco Lamberti[4,5 *]

[1] Division of Physics and Applied Physics, School of Physical and Mathematical Sciences, Nanyang Technological University, 21 Nanyang Link, Singapore 637371, Singapore

[2] Computational Laboratory for Hybrid/Organic Photovoltaics (CLHYO), Istituto CNR di Scienze e Tecnologie Molecolari (ISTM-CNR), Via Elce di Sotto 8, 06123 Perugia, Italy

[3] CompuNet, Istituto Italiano di Tecnologia, Via Morego 30, 16163 Genova, Italy

[4] Department of Information Engineering, University of Padova, Via Gradenigo 6/B, 35131 Padova, Italy

[5] Interdepartmental Centre Giorgio Levi Cases for Energy Economics and Technology, Via Marzolo 9, 35131 Padova

[6] Istituto per lo Studio delle Macromolecole (ISMac-CNR), Via Bassini 15, 20133, Milano, Italy

[7] Institute of Physical Chemistry and Center for Materials Research (LaMa), Justus Liebig University Giessen, Heinrich-Buff-Ring 17, 35392 Giessen, Germany

* Corresponding authors: tzechien@ntu.edu.sg; teresa.gatti@phys.chemie.uni-giessen.de; francesco.lamberti@unipd.it

Abstract

Lead halide perovskites (LHPs) have been for a decade and still remain the rising stars in current materials science research. After ten years of incessant work, researchers have reached important results in LHP photovoltaics, overcoming the 24% power conversion efficiency threshold and thus closely approaching silicon performance. On the other hand, challenges are now open for finding other useful applications for LHPs, going beyond the prevalent use in low-cost solar cell technologies. To this goal, the multiple possibilities which can be explored rely on the modification of the lattice structure of LHPs, creating libraries of different compounds with different peculiar properties. In this review, we conducted a deep and comprehensive examination of the recent literature reporting on two main strategies for making alterations at the native LHP structure. We defined them, namely, the endogenous and exogenous strategies. The first one accounts for all the compositional engineering methodologies that were applied during the last 10 years for the internal modification of the LHP lattice, while the second one refers to the realization of nanocomposites, in which LHPs and other materials are combined together. The review encompasses historic, theoretical, spectroscopic,

electrical and technological contents, in order to provide a comprehensive starting point for defining a new era in LHP research.

Keywords

Lead halide perovskites, compositional engineering, doping, nanocomposites

List of abbreviations of common words used in the text

CB	Conduction band
DFE	Defect formation energy
DFT	Density functional theory
DOS	Density-of-states
FAI	Formamidinium iodide
IS	Impedance spectroscopy
LED	Light-emitting diode
LHP	Lead-halide perovskite
MAI	Methylammonium iodide
MAPI	Methylammonium lead iodide
MOF	Metal organic framework
NC	Nanocrystal
NP	Nanoparticle
NPL	Nanoplatelet
PCE	Power conversion efficiency
PD	Photodetector
PL	Photoluminescence
PLE	Photoluminescence excitation
PLQY	Photoluminescence quantum yield
PSC	Perovskite solar cell
PV	Photovoltaics

PVK	Perovskite
SEM	Scanning electron microscopy
TAS	Thermal admittance spectroscopy
VB	Valence band
VBM	Valence band maximum
XRD	X-Ray diffraction

1. Introduction

Within the realm of green technologies, photovoltaics (PV) has reached a high level of technological readiness. Polycrystalline and thin-film silicon solar cells overcame 21% efficiency after two decades of thoughtful research and engineering, and nowadays they hold the largest share within the solar PV market.[1] Emerging solar technologies (*i.e.*, the so-called third-generation solar cells)[2] are potential game-changers, which would decrease installation costs and redefine the entire economy and manufacturing of the PV market. However, these technologies are still struggling with low long-term stability in terms of performances, *i.e.*, a shelf-life for solar cells of some weeks compared to years for conventional silicon-based ones. Hence, more focused efforts are needed for third-generation PV to be realistically competitive with silicon PV.

Among these emerging PV technologies, perovskite solar cells (PSCs) gave a substantial new impetus to the field,[3,4] with the possibility of realizing tandem solar cells between perovskite layers and silicon thin-film devices. In a couple of years, the efficiency has surged from 21 to 28%,[4,5] that is to-date the record value for emerging PV and close enough to the junction Si theoretical limit (29%), by exploiting the two different solar light working window (the near-IR region with Si and the UV-visible region with perovskites). Furthermore, given their peculiar photophysical properties, hybrid lead halide perovskites (LHPs), as the active components of PSCs, have transcended the PV field and brought innovation in other technological applications, ranging from light-emitting diodes (LEDs)[6,7] to light detection,[8] piezoelectrics,[9] thermolectrics[10] and photocatalysis.[11]

The inherent defectivity[12] of the methylammonium lead iodide (MAPI) perovskite (a sort of benchmark material for LHPs), deriving from the hybrid organic-inorganic nature and being significantly higher than that of silicon (defects concentration of 10^{18} cm^{-3} for MAPI *vs* 10^{17} cm^{-3} for polycrystalline silicon and 10^{14} cm^{-3} for monocrystalline silicon) is the key limitation of these emerging PV materials. Theoretical and experimental works show that the energy traps due to lattice

Commentato [MR1]: A useful citation could be this book DOI: 10.5772/821 and these papers https://doi.org/10.1063/1.1618912 DOI: 10.1002/pssa.201200216 DOI: 10.1016/0038-1098(75)90284-7

Maybe we can ask to Daniele?

disorder, placed inside the band gap and acting as charge recombination centers, oblige researchers to improve the crystalline quality of the material by passivating bulk and surface defects.

One possible experimental strategy toward defects-control and engineering is to combine LHPs with other materials having peculiar characteristics and this goal can be achieved in two main different ways, as depicted in Figure 1): i) endogenously by compositional modification of the LHP crystal lattice and ii) exogenously by mixing LHP with other species into nanocomposites.

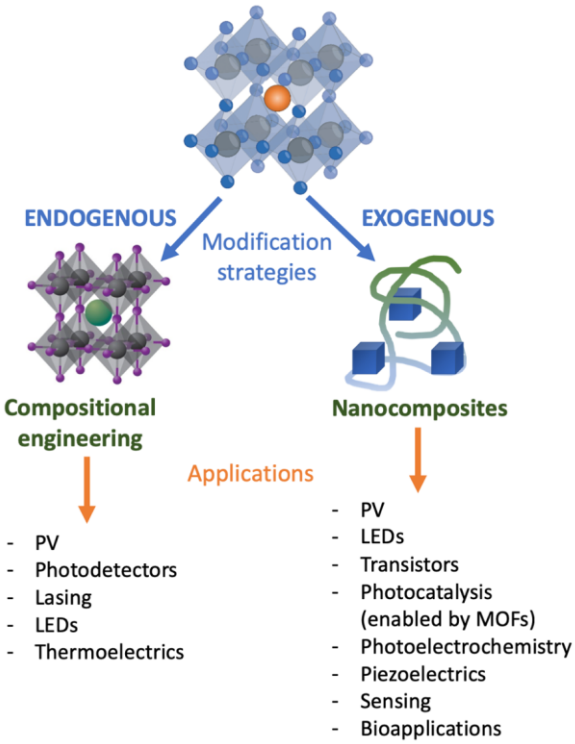

Figure 1. Modification strategies for LHPs, as surveyed in this review. Endogenous and exogenous methodologies are distinguished and target applications for the modified LHPs are indicated.

The first type of modification accounts for all the experimental approaches leading to variations in the MAPI crystalline structure, such as the use of different organic/inorganic cations (formamidinium, Cs), the use of various halides (iodide, bromide, chloride), the introduction of heteroatoms for chemical doping and the reduction of perovskite (PVK) dimensionality by introducing bulkier

cations. Within the second type of modification, we include all the strategies to fabricate nanocomposites based on LHPs, i.e. by interfacing them with polymers, molecular materials or other inorganic/hybrid materials.

Considering the nowadays tremendous impact of LHPs beyond the PV field (see Figure 1), the effort for coupling them with other material is crucial and will likely be the focus of PVK research in the upcoming years.

Herein, we want to provide a comprehensive and thoughtful overview not only of these strategies but also of the physical and technological consequences arising when coupling LHPs with other materials. Indeed, this review will encompass and unify theoretical, spectroscopic, electrical and technological perspectives of LHP combination with other species, by highlighting in a critical way the most relevant examples present in the literature and discussing future perspectives.

2. Endogenous strategies

2.1. A short chronology of LHPs compositional engineering

The paramount versatility of LHP chemistry depends largely on the intriguing properties of the PVK lattice structure. The general chemical formula of a PVK is ABX_3, where A^+ and B^{2+} are two positively charged ions (cations) and X^- is a negatively charged ion (anion). The cubic phase is the hallmark of the PVK structure. Within this arrangement, a large A^+ cation is contained in the center of a cube, on whose vertices are displaced eight B^{2+} cations. Moreover, each of these B^{2+} cations coordinate six X^- anions in an octahedral arrangement. The Goldschmidt's tolerance factor (t) establishes a geometrical criterion for defining the structural stability of a PVK structure for different combinations of A, B, and X ions, on an empirical basis. Notably, it can be used as an indicator of the distortion of the crystal structure:[13]

$$t = \frac{r_A + r_X}{\sqrt{2}(r_B + r_X)}.$$

where r_A, r_B and r_X are the radius of A-cation, B-cation and X-anion, respectively.

For values of *t* in the 0.8-1.0 range, the structure of the PVK will be preferentially cubic. On the contrary, when *t* is higher than 1.0 or lower than 0.8, the PVK structure will be unstable, and other non-PVK structures will be formed.[14]

The first organic cation used to build an LHP structure, in combination with Pb^{2+} and Br^- or I^-, was the methylammonium ion $CH_3NH_3^+$ (abbreviated to MA^+).[15–17] As the size of the A-cation is increased, an expansion of the crystal structure and a decrease in the bandgap are expected, thereby gaining a favorable red-shift of the absorption onset:[18] for this reason, formamidinium $[CH(NH_2)_2]^+$ (FA^+)[19] and cesium (Cs^+) have been introduced.[20] However, experimental evidence shows that LHP materials with a single A-cation suffer from thermal and structural instability.[21] To overcome these limitations while at the same time optimizing the bandgap for the use in optoelectronic devices, mixtures of MA^+, FA^+, and Cs^+ are used. For example, a mixture of MA^+ and FA^+ is used to boost the solar light harvesting within the active material having the theoretical formula $MA_xFA_{1-x}PbI_3$. In addition, cations like Rb^+ and Cs^+ have been demonstrated to be useful tools for synergistically reduce defects and recombination losses, by improving the overall charge transport in the LHP.[22] The main issue to be resolved in this type of LHP architectures is to avoid the formation of the undesired δ-phase for $FAPbI_3$ with poorer optoelectronic properties[23] and to obtain higher values for power conversion efficiency (PCE) in solar cells.[24] For this reason, other strategies were found to be more effective, such as the mixing between FA^+ and Cs^+ in $Cs_xFA_{1-x}PbI_{3-y}Br_y$, that improves both the thermal stability of the material and the bandgap.[25] After the double-A-cation, the triple-A-cations LHP with Cs^+, FA^+ and MA^+ was further developed, as in a complex species like $Cs_x(MA_{0.17}FA_{0.83})_{1-x}Pb(I_{0.83}Br_{0.17})_3$. By employing this formulation, the PCE of PSCs reached for the first time the outstanding value of 21.1%.[26] Finally, by introducing the fourth cation, Rb^+, in the crystal lattice, the efficiency and stability of PSCs were further increased, and the performances remained stable for almost 500 hours during the continuous device operational activity.[27]

For the purpose of this review, the metal B-cation considered will always be lead (Pb^{2+}). It is worth mentioning anyway that, with a huge effort, the scientific community is trying to completely or

partially substitute lead to produce lead-free or quasi-lead free PVK materials, possibly complying with RoHS, EWRA and other international directives on hazardous substances regulation.[28–34]

Another very active field within the contest of LHPs compositional engineering is the improvement of structural stability via heteroatom doping, *i.e.*, the substitution of both the A and B cations. Interesting results were obtained by doping LHPs with Mn and Sr elements, that also partially substitute Pb in the crystal structure in cubic $CsPbI_3$.[35,36] In general, metal replacement induces significant changes in the chemical bonding effects and optoelectronic properties of LHPs.

The X position is occupied by anions, usually halides. The possible halides are chloride (Cl^-), bromide (Br^-) and iodide (I^-). In addition, a mix of the halides can be tolerated in the crystal structure and this is also a powerful strategy to tune the LHP band gap.[37] In a recent paper,[38] Zhu et al. have discussed the role of lattice strain in mixed cation/anion LHP structures generated after compositional separation/thermal stress[39,40] and caused by the chemical mismatch among the different constituents and the non-equilibrium growth conditions existing during film fabrication. This simple evidence notably highlights the importance of dealing with structural defects when discussing LHP properties: the presence of defects in the lattice can strongly alter the optoelectronic performance of a semiconductor due to their ability to trap photo-generated carriers and to promote non-radiative recombination processes, by leading to open-circuit voltage and efficiency losses.[41] The chemical nature of charge traps in this class of systems has been widely studied, mainly by spectroscopic and computational techniques. Spatially resolved PL experiments performed on polycrystalline films of MAPI showed that I-rich surfaces are less emissive than Pb-rich surfaces, suggesting that most of the charge traps form in I-rich portions of the LHP.[42,43] This result is also related to the study reported by Minns et al., who showed that high structural disorder in bulk MAPI is associated with iodine interstitials, through X-ray and neutron diffraction techniques.[44]

Also, the interaction with external agents like oxygen represents an alternative path to doping in tuning the optoelectronic properties of LHPs. The exposure to low oxygen pressures improves reversibly the associated PLQY,[45–51] confirming a direct effect of passivation of the charge traps,

Commentato [TG2]: add ref: DOI:10.1039/C8SE00143J

Commentato [TG3]: add same ref as above.With these two we reply to rev 1 request of citations number 3

as will be deeply discussed further in the text. For the sake of completeness it is important to mention that X-ray photoelectron spectroscopy (XPS) experiments revealed the high tendency of MAPI to release MAI from the lattice through the formation of Schottky defects, such as V_{MA} and V_I, but also Pb metal clusters, with potentially harmful impact on the overall PL properties:[52] this indeed confirms the intrinsic low stability of the LHP lattice.

To improve the stability of the LHP structure, also Eu^{3+} - Eu^{2+} ions were added, as redox shuttle additives, with the double aim of both oxidizing atomic lead and reducing molecular iodine, which acts as recombination and degradation centers. With the presence of europium cations, Wang et al., showed the possibility to reach up to 21% in the solar cell device with stable performances in the maximum power point tracking up to 500 hours.[53]

Recently, post-synthesis processes aimed at passivating charge traps in pristine LHPs have also been carried out.[54–56] In these works, polymers, nano-composites and small molecules were added directly on the LHP layer to passivate the recombination centers, decreasing the non-radiative losses in LEDs and improving the performances of PSCs. These aspects regard anyway the strategy we have defined as exogenous and will be therefore discussed later in the text.

Finally, if the A cation is big enough, the 3D LHP cannot form and the result is a 2D or a quasi-2D LHP structure. These kind of perovskites are usually more resistant to humidity[57,58] and can be a good solution to overcome the stability issues in PSCs.

2.2. Theoretical framework: computational modelling of point defects

From an experimental point of view, LHP doping strategies are commonly carried out by a trial and error approach, with prediction possibilities left to the intuition and experiences of the scientist. Reversing this picture, *i.e.*, realizing LHP materials-by-design on a microscopic modelling basis, would result in a paradigm shift for LHPs research. In this regard, the use of computational techniques based on the density functional theory (DFT) represents a reliable method to study the thermodynamic stability and defects processes in solids.

Within the DFT framework, the modelling of defects is usually carried out by using supercells in periodic boundary conditions. The stability of a defect in the lattice is estimated by calculating the associated defect formation energy (DFE) with the general equation:[59–61]

$$DFE(X^q) = E(X^q) - E(bulk) - \sum_i n_i\mu_i + q(E_F + VBM) + E^q \quad (1)$$

where $E(X^q)$ is the energy of the defect supercell of charge q, $E(bulk)$ the energy of the pristine supercell, n and μ are the number, and the chemical potentials of the species and E_F is the Fermi level of the system referenced to the valence band maximum (VBM) of the pristine crystal. The Fermi level of the system is allowed to span the entire bandgap of the LHP. The E^q term is a correction including the shift of the electrostatic potential and the periodic interaction of the charges. According to equation 1, DFEs are functions of the chemical potentials and the Fermi level of the system. By the analysis of DFEs and their variation *vs* the Fermi level it is possible to predict the stable states of charge of native defects in a particular range of Fermi level, as well as their density by applying the Boltzmann law $c(D^q) = N_s \exp(-\frac{DFE(D^q,E_F)}{kT})$, where N_s is the density of the defects sites in the modeled supercell, T is the absolute temperature and k the Boltzmann constant. Once the densities of the different defects species are calculated it is possible to estimate the intrinsic Fermi level of the system by solving the associated electro-neutrality equation. The thermodynamic ionization levels (TIL) between different charge states q/q' of a defect are defined by the expression

$$\varepsilon(q/q') = \frac{DFE(D^q,E_F=0) - DFE(D^{q'},E_F=0)}{q'-q} \quad (2)$$

where DFE (D^q, $E_F = 0$) are the formation energies of defects in the state of charge q calculated for $E_F = 0$, *i.e.* at the top of the valence band (VBM).[59] TILs represent the Fermi energies (E_F) where the DFEs of a defect species in different charge states are equal DFE (q',E_F) = DFE (q,E_F), *i.e.* the crossing points between the DFEs lines. Ionization levels thus represent the redox potentials associated to the ionization of a defect, referred to the VBM of the perfect crystal.

Defects with ionization levels close to the band edges of the pristine crystal by few meV are stable in a single charge state along the bandgap and are called shallow. The low ionization energies of these

defects lead to the doping of the material. On the other hand, defects with ionization levels deep in the bandgap can exist in different states of charge within the Fermi level range, whose stability can be tuned by tuning the Fermi level itself of the system, for instance through extrinsic doping. According to the Shockley-Read-Hall theory,[62] defects with ionization levels deep in the bandgap can trap photo-generated charges by promoting their recombination on the defect center. The trapping rate is higher on defect centers with ionization levels placed in the middle of the bandgap, while shallow defects are mostly inactive in the process.[62]

One of the advantages of equation 1 is that different values of chemical potentials can be assigned to elements to simulate different conditions of growth of the LHP. Halide or metal rich conditions can be simulated by fixing the chemical potential of a species to its value in the standard state and by solving chemical equilibrium for other components to preserve the thermodynamic stability of the LHP. In doping processes, the chemical potential of the extrinsic element may be assigned by including in the equilibrium conditions the limit of solubility of the dopant and the formation of the closest thermodynamic stable phase.

A critical aspect for an accurate estimation of DFEs is a quantitative prediction of the band edges energies of the perfect crystal that enters the electronic term in equation 1. DFT calculations in solids are usually carried out by using semi-local functionals, like the Perdew-Burke-Ernzherof (PBE) functional,[63] which provide reasonable estimate of the thermodynamics processes in solids. However, such functionals are inadequate in the description of the electronic structure, by leading to a systematic underestimate of the band gaps. The PBE functional predicts a bandgap for MAPI of 1.56 eV but, although in good agreement with experiments (E_g = 1.60 eV), such matching is only fortuitous.[64,65] The inclusion of spin-orbit interactions, particularly important in the simulation of heavy elements like Pb, leads to a remarkable narrowing of the bandgap to a value of 0.5-0.6 eV.[66,67] This last value should be considered the effective bandgap calculated by the PBE functional, and it highly underestimates the experiments. State of the art GW calculations (including SOC) predicted a bandgap of 1.64 eV[64] for MAPI, by confirming that a quantitative description of

the electronic properties of perovskites can only be achieved by using methods beyond semi-local functionals. In this regard, the use of hybrid functionals, like PBE0 and HSE06,[68,69] represent a good compromise between computational cost and accuracy and so far they are among the most accurate methods for the calculations of defects properties in this class of systems. Notably, the use of semi-local functionals without including spin-orbit effects and self-interaction errors leads to uncertainties also in the identification of geometry minima, particularly for localized states and open-shell defects.[70] Although computationally more expensive, the use of hybrid functionals even in the geometry relaxations of defects should be the preferred choice. Other techniques based on DFT+U schemes, however, have also been explored.[71]

2.3. DFT simulations of doping processes in LHPs

Doping of the metal is an effective strategy to increase the stability of the lattice of a perovskite phase, as showed for the case of $CsPbI_3$ that we nominated earlier in the text .[35] This perovskite is not stable in the alpha form, but the partial replacement of Pb^{2+} by isovalent substitution with Mn^{2+} is an effective strategy for the stabilization of the $CsPbI_3$ active phase. DFT calculations confirmed that Mn alloying induces an increase of the cohesive energies of the phase to the value of 0.1 eV/f.u. in the mixed $CsPb_{0.5}Mn_{0.5}I_3$ phase, with configuration entropy further favoring the process.[35] The study of the electronic structure of this alloy phase highlighted that electronic states of Mn are not coupled to the band edges, thus preserving the intrinsic electronic structure of the pristine LHP (see Figure 2a). This confirms that isovalent substitution of lead by other metals with similar ionic radius can stabilize the lattice without altering the optoelectronic properties of the PVK. The absence of electronic states of the dopant near the band edges (and in the band gap) prevents the unintentional formation of charge traps in the material, which can have detrimental effects on the efficiency of a PSC.

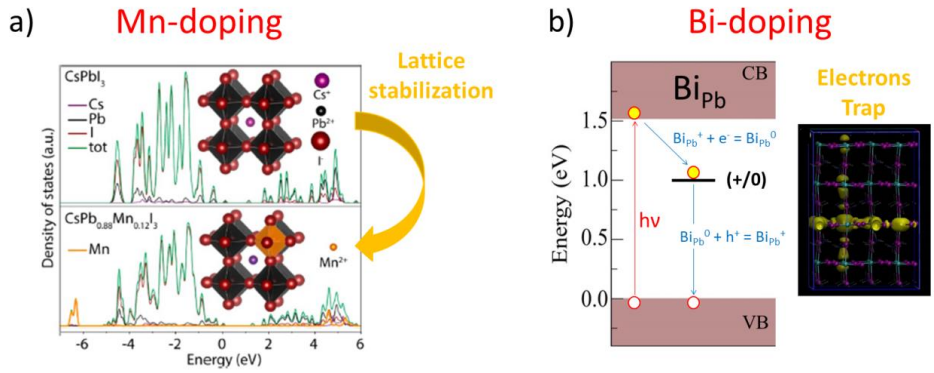

Figure 2. a) Structure and atoms projected electronic density of states (PDOS) of pristine and Mn-doped cubic $CsPbI_3$; b) Electron traps introduced by Bi-doping in the bandgap of pristine MAPI. Reprinted and adapted from ref [35] and ref[72]. Copyright 2017 and 2018 American Chemical Society.

This aspect is particularly critical in doping strategies using aliovalent metals, as shown in the case of Bi-doping of MAPI. Mosconi et al. investigated by hybrid DFT the TILs associated to the Bi center in MAPI, by showing that incorporation of Bi in substitutional position to Pb leads to the formation of deep electrons charge traps in the band-gap, placed at ~1.0 eV above the VB (see Figure 2b). This result allowed to understand the origin of the bandgap narrowing and PL quenching observed in Bi-doped LHPs.[72]

The beneficial effects of doping in reducing intrinsic charge traps of the pristine LHP is a particularly important issue. Several DFT works have investigated native defects in perovskites .[12,13,54-65,67-80] A predominance of shallow defects such as Pb vacancies (V_{Pb}), MA interstitial (MA_i) and iodine interstitial (I_i) defects have been reported by DFT studies in $MAPbX_3$ LHPs, with X= I, Br and Cl.[73] Similar results have also been reported for $FAPbI_3$ and inorganic LHPs.[74–76] Walsh et al. discussed that Schottky defects, *i.e.*, V_{MA} + V_I, are among the most stable defects couple in MAPI and their formation does not lead to alteration of the associated optoelectronic properties.[77] Notably, all these studies have been carried out by using semi-local functionals. Other studies based on hybrid functional DFT highlighted the emergence of deep trap states in the LHP, primarily associated with

uncoordinated iodines.[78,79] In Figure 3, the defects formation energies and thermodynamic ionization levels diagrams of native defects in tetragonal $MAPbI_3$ are reported as calculated by using the hybrid HSE06 functional, SOC included. As showed by diagrams, although many native defects have a shallow character, I_i and V_{Pb} introduce deep levels in the band gap of the LHP.[78] I_i can trap both holes and electrons through the (0/-) and (+/0) levels placed at ~0.30 and ~1.0 eV above the VB, respectively, while V_{Pb} can trap holes through the (2-/-) transition at ~0.1 eV above the VB. These defects are thermodynamically stable in the – and 2- state of charge, respectively, at the Fermi level and share a very similar defect chemistry.[60] The study of diffusion coefficients of native defects in the MAPI lattice highlighted that iodine ions move faster than MA ions, which in turn move faster than Pb, with calculated barriers of ~0.1 eV, 0.2-0.5 eV and > 0.8-1 eV for these species, respectively.[80,81] Based on these results a prominent activity of I_i upon the photo-excitation process is expected, while V_{Pb} likely play only a limited role due to the relatively shallow character of the (2-/-) transition and the high migration barrier.

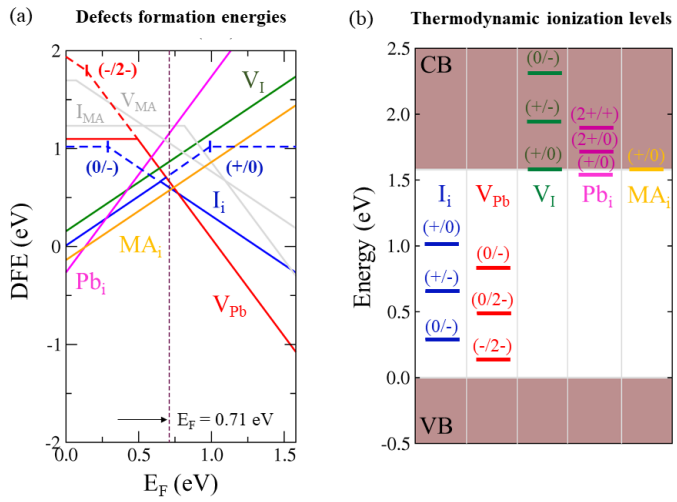

Figure 3. a) Defects formation energies diagram of native defects in tetragonal MAPbI3 calculated at the HSE06-SOC level (dispersion corrections included) in the 2x2x1 supercell and b) associated thermodynamic ionization levels diagram. Adapted from ref [78] with permission of The Royal Society of Chemistry.

Changes in defects and PL properties of LHP upon doping and when interacting with the environment have also been studied computationally. Shi et al. performed an extensive DFT study about the doping activity of several extrinsic elements in MAPI, by concluding that the p-type doping with Na, K, Rb, Cu, and O elements is more accessible than n-type doping.[82]

Potential charge traps healing strategies based on isovalent halide doping with Br and Cl in MAPI have also been proposed by some of us.[78] As reported in Figure 4a, the partial replacement of I_i with more stable Br and Cl interstitials leads to a shallowing of the (0/-) ionization level, responsible of the holes trapping, by passivating the defect center. Other DFT works confirmed the beneficial effects of isovalent halide doping with Br and Cl, by showing that these elements can effectively passivate charge traps and increase the lifetimes of charge carriers in MAPI.[78,83]

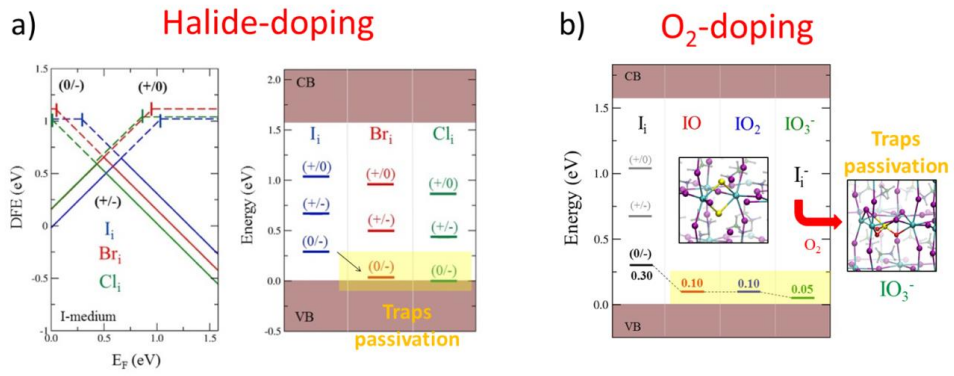

Figure 4. a) Effects of isovalent halide-doping on the trapping properties of iodine interstitials. Adapted from ref [78] with the permission of the The Royal Society of Chemistry; b) Effects of oxygen doping on iodine interstitials traps. Adapted with the permission from ref [84]. Copyright 2017 American Chemical Society.

The effects of LHPs exposure to external agents such as iodine and oxygen gas have been discussed with emphasis on the impact of these agents on the charge traps formation and healing.[84,85] In a mechanism discussed by some of us, the exposure of LHPs to limited quantities of molecular oxygen may induce the oxidation of negative iodine interstitials to form molecular IO_n^- species leading to a shallowing of the (0/-) transition, similarly to isovalent halide doping.[84] Oxygen, and particularly

water, however, can also activate photo-degradation paths in $MAPbI_3$, through the formation of superoxides species, as discussed by Aristidou et al..[86]

On the other hand, PL quenching of $MAPbI_3$ is expected, due to the exposure to I_2 vapors. As discussed in Meggiolaro et al., the high chemical potential of iodine in the gas phase leads to an increased density of I_i and V_{Pb} charge traps in the LHP, with consequent *p*-doping and detrimental effects on the PLQY.[85]

2.4. Engineering of LHPs optical properties through endogenous modifications

The combination of an electronic structure dictated by the $[PbX_6]^{4-}$ building blocks together with the ionic nature of Pb-X bonds underlies the uniqueness of LHPs, as a platform for compositionally tailored optical properties.[87] Within these building blocks, the valence band maximum and conduction band minimum are composed by σ-antibonding states of Pb 6s-X 5p and Pb 6p-X 5s, respectively.[64,88] Thus, LHPs optical properties can be primarily tuned by doping this structure, *i.e.*, by partially changing the composition of these building blocks. Although the extreme versatility of the LHP chemical structure allows to intervene on each component, as previously described, changes in halide anions X^- are by far the most commonly used strategies to tune the electronic structure near the band edges, as differences in halide atoms dielectric constant have profound effects on the resulting excitonic properties of the material.[7,89,90] Indeed, as widely explained in Section 1.1, the replacement and alloying of A^+ cations has been explored to tailor both the stability of these materials[91–94] and the hot-carrier cooling properties.[95,96] The reduced impact of the A^+ cations on the optical properties of LHPs stem from their marginal role in the band structure, which confines them mostly to their geometrical role, although the discovery of some dielectric effects on the electronic excitations (*i.e.*, dielectric drag and screening) suggest a possible pivotal role played by these moieties.[97,98] Since its inception, replacement of the B^{2+} cation aroused much interest for lead-free LHPs.[99,100] Alloying strategies regarding the B^{2+} cation offers a broad tunability of LHPs optical properties, but this often impacts the electronic dimensionality of the material, thereby resulting in a defect-intolerant electronic structure and therefore in poor optical and carrier transport

properties.[101,102] Hence, this doping strategy is inherently more complex, invoking considerations on geometrical, electrochemical, and electronic aspects, and therefore will be discussed in detail in the following paragraph. Noteworthy, when coping with some structural stability consideration, the unique versatility of LHPs solid-state chemistry potentially allow for a simultaneous application of the doping strategies already described.

Although other reviews in this field present the different strategies of doping in terms of which building block (A, B, or X) is substituted, we believe that a better description can be given in terms of processes.[103,104] Among the various opportunities offered by LHPs to tune the optical properties via doping, two approaches relying on different processes can be adopted: (i) bandgap engineering; (ii) down-conversion and quantum cutting. While the first approach aims at intervening on the electronic band structure by continuously shifting energy levels through progressive halide doping, the second approach introduces heteroatoms whose localized levels act as color centers within the LHPs matrix.

2.4.1. Bandgap engineering

A full composition-driven tunability of the optical properties of LHPs has been demonstrated for the $AB(X_{3-x}X'_x)$ systems, in which halide doping allowed tuning the energy gap across the whole visible spectrum. In 2013 Seok et al. reported the realization of a solid-state solution of alloyed $MAPb(I_{3-x}Br_x$, x=0-1) with photoluminescence (PL) peak (2.28-1.57 eV) linearly dependent on the bromide content (Figure 5a).[105] Sum et al. demonstrated the full visible range optical tunability of thin films up to 3.2eV of MAPb(Br3-xClx) for thin films, while Zhu reported tunable lasing for LHPs nanowires (Figure 5b and c).[106,107]

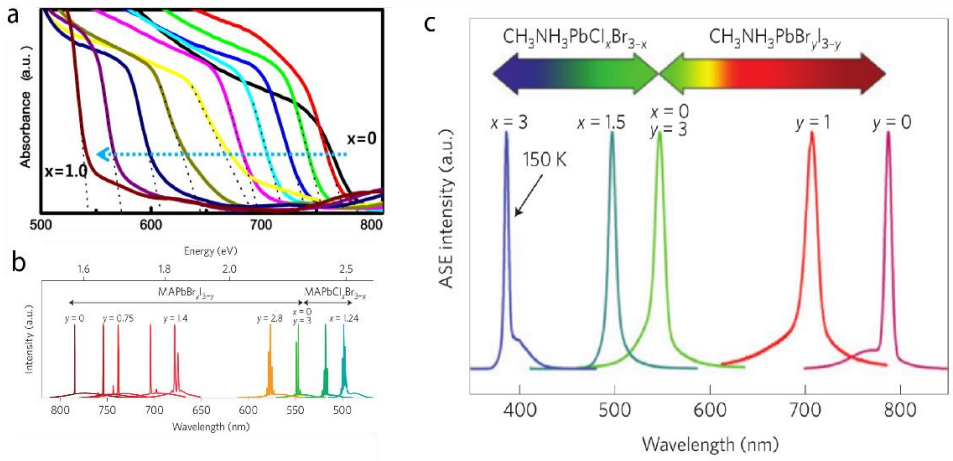

Figure 5. a) Visible absorption spectra of $MAPb(I_{1-x}Br_x)_3$, the increasing amount of Br^- anions cause a blueshift in the absorption spectrum. Reproduced with permission from Ref [105]. Copyright 2013 American Chemical Society. b) Tunable lasing emission from $MAPb(I_{1-y}Br_y)_3$ and $MAPb(Br_{1-x}Cl_x)_3$ nanowires. c) Tunability of PL and amplified spontaneous emission (ASE) for $MAPb(I_{1-y}Br_y)_3$ and $MAPb(Br_{1-x}Cl_x)_3$ thin films. Reproduced with permission from Ref [106]. Copyright 2014 Springer Nature

The substitution of iodide anions with smaller bromides affects the perovskite lattice constant, thereby determining a transition from the cubic phase to the tetragonal phase. Thus, halide doping strategies cannot overlook structural effects (see Section 1) since these strongly impact the optical properties, for instance via the Rashba effect, *i.e.*, the spin-dependent momentum splitting of degenerate bands.[108,109] Qi et al. demonstrated the existence of an optimal substitution ratio for Cl doping of $MAPbBr_3$ dictated by the interplay between Pb-halide bond strength and strain considerations,[110] as previously shown theoretically by Wei et al.[111]. Thus, the use of small quantities of Cl doping in $MAPbBr_3$ has allowed Huang et al. to achieve a high mobility-lifetime product in $MAPbBr_{2.94}Cl_{0.06}$ single crystals and demonstrate their use as gamma-ray detectors under bias.[112]

The substitution of I with Cl is still a matter of debate: despite resulting in charge mobility increases, no general consensus has been reached on the role of Cl and its solid-state chemistry in the perovskite lattice. Indeed, conversely from Cl/Br and Br/I, Cl and I present very low miscibility (below 4%)

mostly due to the structural considerations, thereby preventing their practical use for the tuning of optical properties and casting doubt on its real role. Snaith et al. introduced the incorporation of chloride anions in 2012 [113] and led Stranks and coworkers to the discovery of the outstanding 1um carrier diffusion lengths, [114] to 10-fold greater with respect to the groundbreaking discovery by Sum et al. on bare MAPI.[115] A common explanation for the increase in carrier mobilities upon chloride doping hinges on possible passivating effect of these ions on the hole traps formed at the grain boundaries. [DOI: 10.1002/aelm.201500044 Nevertheless, we believe that more work is needed to provide a more comprehensive picture of the role played by chlorine (*e.g.*, structural, morphologic) and its relation with the improvements in devices' performances.[116,117]

As mentioned in previous sections, the doping of A cations has mainly structural effects. Therefore, when a larger organic cation L is introduced, the dimensionality of LHPs is tuned down to 2D, and the different physics drives different degrees of white light emission, as shown in 2014 by Karunadasa.[118] Here, the dimensionality reduction further emphasizes the role of electron-phonon coupling in these materials. While the presence of a moderate e-phonon coupling has been thoroughly investigated in bulk LHPs, [doi:10.1038/ncomms11755] its role in lower dimensional perovskites has been demonstrated only more recently [doi:10.1021/acs.chemmater.9b02267] and its fine tuning opens to new exciting opportunities for tailoing these materials' properties[doi:10.1038/s41563-018-0081-x]. For an introduction to the optical properties of these systems the reader is referred to Reference [119], and Reference [10.1016/j.trechm.2019.04.003].

Commentato [MR4]: I added the polarons here, I believe it is the only place where it would not disrupt the flow

In LHPs quasi-0D nanocrystals (NCs) the concept of anion doping is taken to the extreme for two different reasons: (i) the lower importance of structural constraints; (ii) the versatility of the colloidal synthesis and the discovery of solution-based anion exchange methods. Starting from ligand assisted re-precipitation (LARP) synthesized 5-20 nm size $MAPbBr_3$-NCs, Song et al. reported an efficient alloying by the introduction of MAI and MACl solutions in isopropanol.[120] The alternative approach by direct LARP synthesis with mixed precursors solution of alloyed $MAPb(X_{3-x}X'_x)$-NCs was developed by Zhang et al. in 2015[121], while a few months later Protesescu et al. introduced

the alloying in the hot-injection synthesis of $CsPb(X_{3-x}X'_x)$, with extremely high PLQY between 50 and 90%.[122] Ultimately, the post-synthetic anion exchange for Cs-based nanocrystals was introduced [123,124] and demonstrated the mutual exchange of anions between different nanocrystals, thereby revealing the high mobility of halides anions in perovskite nanocrystals. In recent years, the post-synthetic anion exchange has been widely studied, and many precursors were developed, achieving a complete tunability of the optical properties of the nanocrystals.[125–129]

This strongly dynamic nature of halides underlies one of the most severe limitations in the stability of anion-alloyed LHPs: the photoinduced halide segregation sometimes called the Hoke effect.[130,131] The presence of ion migration, already addressed in pure MAPI by De Bastiani et al.,[132] was revealed to be one of the key factors driving the segregation of halide rich phases in perovskites and lately confirmed by from some of the authors.[133] Herz et al. have recently demonstrated the presence of a direct link between halide segregation and weight of the trap-mediated recombination in the film.[134] For a complete description of these effects the reader can refer to the review by Kamat, who pioneered this field.[135]

Besides the mere tuning of optical transition energies, the halide exchange profoundly impacts the underlying photophysics of LHPs, and, more specifically, their excitonic properties. The nature of LHPs lowest-energy excited states is crucial for their applications since the light-emitting application necessitate bound excitons to outpace the trap mediated recombination ($\propto n$). On the contrary, PV applications prefer loosely bound excitons. The parameter better quantifying the strength of the interactions between the electron and the hole is the exciton binding energy, usually extracted by Elliott model fitting of the absorption spectrum.[136,137] Iodide based LHPs have been reported to display exciton binding energies ranging from 6 to 40 meV (with a marked dependence on sample preparation and measurement techniques).[138] Using LHPs with low binding energies allows for PV applications, since free carries are easily generated within the active layer due to easily splitting of the excitons; therefore these LHPs should belong to the class of free-charge semiconductors.[139] On the other hand, the anion doping mainly reduces the dielectric constant of the medium, thereby

resulting in higher binding energies and therefore “more excitonic” materials. Accordingly, reported values for bromide LHPs ranges from 70 to 160 meV, while for chloride reported values are around 70 meV.[138] Hence, anion alloying is not only a viable strategy to tune the energetic levels, but it also allows a fine-tuning of the excitonics of these materials.

2.4.2. Down-conversion and Quantum-cutting

Although compositional doping allows an outstanding degree of tunability on the optical properties, each tuning strategy should face the main setbacks that can limit their large-scale and long-term applications. Among others, the potentially undesired phase transitions, anion segregation, and reduced stability above the optimal doping concentration limits are the most important ones.[135]

An alternative approach encompasses the intentional introduction of limited amounts of heteroatoms during the synthesis of the LHPs and is thereby focused on the partial replacement of Pb^{2+} cations. This strategy aims to modulate not only the optical but also optoelectronic and magnetic properties of the LHPs without affecting their basic structural properties.

Notably, the heteroatom doping has been mostly applied to LHPs nanocrystals and therefore has primarily benefited from the amount of knowledge developed for II-VI semiconductor quantum dots in the past 30 years.[140] As described in the recent review by Bakr, the introduction of heteroatoms within LHPs has focused on metal cations, and their successful introduction has been demonstrated for both isovalent (B^{2+}) and aliovalent (B^{+} or B^{3+}) metal cations.[141] The rationale for tuning the optical properties of LHPs by substitution with a metal cation can be found by analyzing the relation between the energy levels of the dopants and those of the host material. As discussed in Section 2.3 metal dopants with electronic states coupled to the band edge of pristine perovskite alter the associated electronic properties and may potentially introduce defects levels into the band gap, with detrimental effects on the optoelectronic properties of PSC. As discussed by Yin et al.,[142] metals dopants with ionic radii similar to that of lead (e.g., Bi, Ce), preferentially incorporated in substitutional position to Pb, alter differently the fundamental electronic structure leading to PL

quenching/enhancement for Bi / Ce, respectively. Hence, the doping strategies should consider the holistic impact of dopant ions on structure, defectivity and energetic levels of the LHP.

Based on this, we can roughly divide the doping in three main strategies of substitution from the point of view of the resulting optical properties: (i) cations with nearly overlapping energy bands, (ii) cations introducing localized level below the band-edge (shallow traps), (iii) cations introducing energetic levels in the middle of the bandgap of the host material (deep traps). In (i), besides possible energy shifts, the main effects are both the structural effects, such as the defect formation (Section 2.1) and the tuning of the electronic density and properties of the material.[143,144] This will be discussed in Section 3. In (ii) the dopant acts as a color center, receiving energy from the host lattice and realizing a down-conversion. In (iii), provided a suitable energy alignment, the energy absorbed by the lattice can be split between two distinct dopant atoms, thereby achieving above-unity PLQYs. These concepts are summarized graphically in Figure 6 for the sake of clarity.

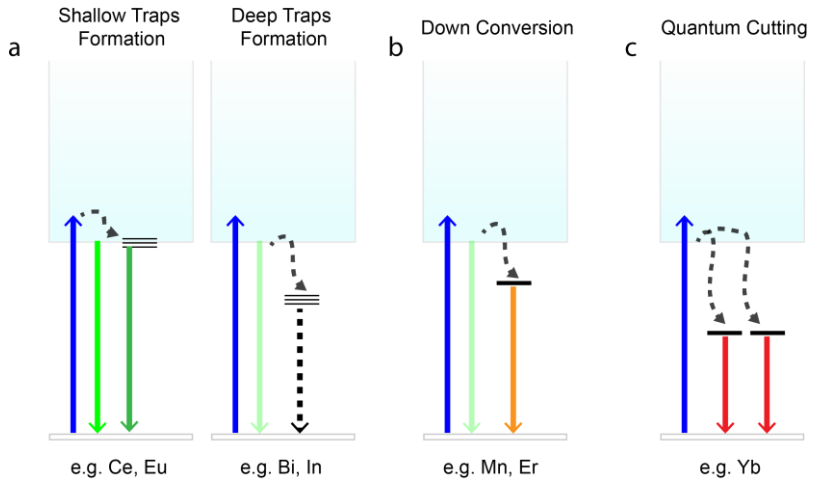

Figure 6. a) Different effects of shallow traps (optically inactive) and deep traps (PL quenching) on the optical properties of LHPs. b) Down-conversion process, where LHPs act as host materials absorbing the excitation and efficiently transferring it to the emissive dopants. c) Quantum cutting process, the quantum of excitation absorbed by the LHP is split and transferred to two dopant ions, providing a resonance condition in the middle of the LHP bandgap.

Hence, besides considering structural effects, the evaluation of the influence of a dopant ion on the optical properties must consider the energy of the electronic transitions between different electronic

configurations, described as a function of the spin S, orbital momentum L and total angular momentum J, as terms symbols $^{2S+1}L_J$.

Gamelin, Norris, and Peng among others have pioneered the introduction of Mn^{2+} in CdSe quantum dots during the 2000s, uncovering exotic effects such as spin-polarized photoluminescence and excitonic magnetic polarons.[140,145–147] The spin-forbidden $^4T_1 \rightarrow {}^6A_1$ transition drives the optical properties of Mn^{2+} in the host lattice.[145] The resulting emission has therefore longer lifetimes ($\sim ms$) and, excitons acquire a magnetic character, thereby paving the way for application in spintronics and in all-optical magnetic switching. Notably, it was the strong interaction between the host lattice and this dopant, demonstrated by Gamelin[147], which raised much interest in applications such as the down-conversion of absorbed light. The defect-tolerant electronic structure of LHPs, overcoming the traping issues in CdSe, made them a perfect candidate for Mn^{2+}doping. [148–156]

The successful Mn-doping of $CsPbCl_3$ and $CsPb(Br/Cl)_3$ LHP NCs was independently reported by Parobek et al. and Klimov et al. in late 2016 and focused mainly on down-conversion applications, thereby choosing chloride and mixed chloride/bromide LHPs given their tunable bandgap.[149,150] The approach proposed by Parobek et al. relies on the introduction of small quantities of Mn salts within the well-established hot-injection synthesis method, developed by Kovalenko.[122] The replacement of Pb^{2+} with Mn^{2+} was confirmed by electron paramagnetic resonance spectroscopy and by $CsPbCl_3$ lattice strain effects on XRD. Even at low doping level <0.2% Mn/Pb atomic ratio, they reported a dual PL, where in addition to the usual excitonic PL (3.08eV) they recorded a broad orange PL peak at 2.1eV ascribed to the spin and parity forbidden transition $^4T_1 \rightarrow {}^6A_1$ of Mn^{2+} excited via energy funneling from the host lattice. Noteworthy, this down-conversion process favorably resulted to outcompete the other non-radiative recombination channels and raising the PL quantum yield (QY) from 1.1% for the bare NCs up to 60% for the doped NCs. The resulting large Stokes shifts make them interesting for applications such as bio-imaging and luminescent solar concentrators. Klimov further extended this approach, by widening the compositional range of doping up to 10%,

subsequently increased by Yang et al.,[148] who acted on the hot-injection temperature to achieve high substitution ratio of $CsPb_{0.54}Mn_{0.46}Cl_3$ NCs while maintaining enhanced PLQYs.

The investigation of different compositions in terms of both halide content and (Pb/Mn) substitution ratio revealed new insights into the host lattice-dopant interaction mechanisms. [152] The observed decrease of dopant emission with increasing Br^- content made clear that the bandgap plays a fundamental role in this process. Zhang et al. confirmed this observation by a systematic halide exchange, where transfer was not detectable for doped Mn:$CsPbBr_3$ and Mn:$CsPbI_3$.[157] The first spectroscopic studies, mostly based on photoluminescence excitation (PLE) and transient absorption (TA), were conducted by Rossi et al. on $CsPb_{0.96}Mn_{0.04}Cl_3$ and reported a slow picosecond energy transfer process $\tau_{ET} = 370\ ps$.[158] Furthermore, this process was reported to be dependent on the Mn^{2+} concentration, reaching down to $\tau_{ET} = 3.6\ ns$.[148,149] Although PLE was useful to identify that the reported dual emission was not originated by different subsets of doped and un-doped dots, the presence of simultaneous dual emission suggested a complicate interaction mechanism.

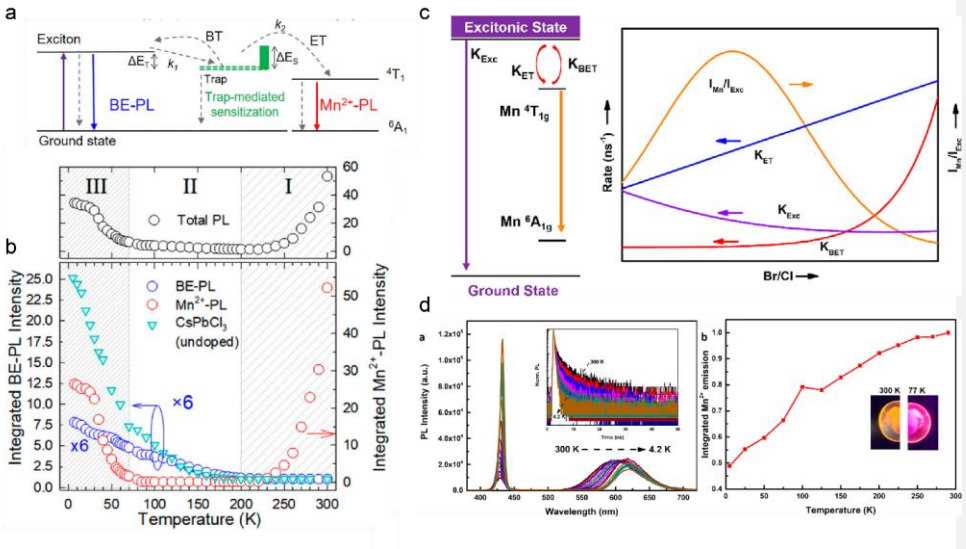

Figure 7. a) Energy levels of the Mn trap-mediated sensitization mechanism, obtained by b) temperature-dependent PL spectroscopy, according to Brovelli et al. Reprinted with permission from ref [151]. Copyright American Chemical Society 2019 c) Energy diagram of Mn-doped $CsPbCl_3$ NCs, comprising energy transfer and back-energy transfer effects

on d) temperature-dependent PL. Reprinted with permission from ref [153]. Copyright American Chemical Society 2018; further permission related to the material excerpted should be directed to the ACS.

Gamelin, Meijerink, and Brovelli reported systematic temperature-dependent PL studies (Figure 7b and d).[151–153] According to the resulting picture, the transfer is likely to proceed via a Dexter-type process, whose resonance condition requires the involvement of an upper ligand-field excited state of Mn^{2+} at the same energy. Furthermore, the presence of dual emission stems from an equilibrium between energy transfer and back-energy transfer, which leads to a branching in the emission, controlled by thermal energy (Figure 7 a and c). Similar energetic schemes have been reported for Mn-sensitized and trap-states in II-VI quantum dots, as well.[145,159,160] Although the consensus on the thermally activated nature of the ET process, with an energy barrier estimated between $\Delta E_{ET} = 105 - 315meV$, the anomalous low temperature (T<50 K) behavior of the Mn^{2+} emission is still under debate (Figure 7b). As shown in Figure 7d, Meijerink reported a constant up to a 5-fold decrease of integrated PL intensity when decreasing T between 300 and 4.2K, and therefore proposed the presence of a long-lived charge-separated state, communicating with the emissive Mn^{2+} $^4T_1$ state.[152,153] Conversely, Brovelli et al. have recently found a different low temperature (T<50K) non-monotonous behavior of the Mn^{2+} PL and have proposed a two-step trap-mediated sensitization mechanism (Figure 7b).[151] According to these studies, the interaction process is not only thermally activated but also is mediated by shallow traps, thereby accounting for the slow energy transfer and the co-existence of exciton and dopant emissions. The resulting Jablonski diagrams for the different interpretations are summarized in Figure 7a and c.

Recently, Congreve and co-workers have reported a brilliant approach to exploit the structural effects of Mn-doping in LHPs NCs to passivate the traps and stabilize the structure. A low Mn-concentration (<0.19%) synthesis $CsPb(Br/Cl)_3$ NCs allowed them to obtain efficient blue emission without having emission from the dopant. The low amount of Mn^{2+} ions resulted in a shorter Urbach tail (from 17.4 to 14meV) and longer excitonic PL lifetimes (from 2 to 3ns), for undoped and doped, respectively. [161]

The effect of Mn^{2+} dopant was investigated on LHP with different dimensionalities (2D and 1D), with similar results, i.e., a dual PL and higher PLQYs.[155]–[156]–[162] Notably, these 2D dimensional colloidal NPLs were used as a reaction intermediate by Son et al. to achieve a direct synthesis of doped Mn:$CsPbBr_3$, improving their optical properties with respect to the anion-exchanged doped NCs.[163]

Although Mn(II) doping has been at the focus of recent investigations, doping with different transition metal cations was successfully reported. The research for Pb-free alternative maintaining a defect tolerance has been driving the exploration of a library of divalent transition metal cations.[99] As demonstrated by Greenham et al., the doping with Sn^{2+} ions not only impact the stability of the perovskites, due to the lower oxidation potential of the couple Sn^{2+}/Sn^{4+} (-0.15V) compared to Pb^{2+}/Pb^{4+}(-1.8V), but also results in poor optical properties in bulk and NCs (0.15% PLQY).[164] For Sn(II), the lower spin-orbit coupling of the 5p orbital compared to Pb(II) 6p, results in a defect intolerant electronic structure, hampering their optical and electrical properties.

Donega et al. demonstrated the doping of cubic $CsPbBr_3$ NCs through a post-synthetic reaction with small amounts (0.15%) of M(II)Br_2 (M=Sn, Cd, Zn) salts.[154] The resulting $CsPb_{1-x}M_xBr_3$ NCs showed a blue shift in the emission properties, ascribed to a lattice contraction caused by the substitutional exchange of Pb^{2+} with smaller radii ions. The linear dependence of the PL position with the lattice vector indicates that introducing small quantities of these ions is a viable strategy to tune the PL, without losing PLQY or stability. Analogously, Bakr, Rogach and Meng have further explored the effect of strain, reporting an increased short-range and therefore quasi-optimal optical properties for LHPs nanocrystals upon the introduction of smaller Ni^{2+}, Cu^{+}, Al^{3+} ions.[165,166] In these cases, the lattice contraction was used to tune the strain, eliminate halide vacancies, and tune the bandgap of the host lattice.

Also aliovalent metal cations have been explored as possible dopants, where the most commonly used ions are Bi^{3+}, In^{3+}, Fe^{3+}, Au^{3+}, Al^{3+}. [157,167–171] As described in Section 2.2, their effects on the LHPs optical properties are determined by the difference in ionic radius, the ligand field

absorption/emission, and the different charge state, which creates defects in the LHPs lattice. Bakr and co-workers demonstrated the efficient bandgap tuning from 540 to 680 nm but a significant PL quenching, upon 10% Bi doping in $MAPbBr_3$ single crystals.[172] The quenching was investigated by Begum et al. in Bi:$CsPbBr_3$ NCs.[169] Upon the introduction of 2% Bi, the PLQY was reported to drop from 0.70 down to 0.08. As demonstrated by De Angelis, Yamada and further confirmed by Snaith, the energy levels introduced by Bi^{3+} ions act as additional non-radiative recombination centers, thereby quenching the PL.[7,72,167,173] Recently, Loi et al. clarified the quenching mechanism in diluted Bi^{3+} doped $MAPbBr_3$ single crystals by steady-state and time-resolved PL measurements.[174] Interestingly, besides explaining the trap-mediated PL quenching, they reported the emergence of a near-infrared PL peak, as a possible result of in-band states emission. Since the most advantageous effects of Au/In/Bi-doped LHPs fall in the realm of the electrical properties (i.e., a shift of the HOMO/LUMO and increase of the charge carrier densities)[175,176], they will be discussed in detail in Section 2.5.

Different from other transition metal ions, which display broad bands and confined to several specific wavelength regions owing to their limited energy structures, lanthanides, and actinides (rare earths, RE) exhibit a much wider range of tunability. The rich and unique photophysics of RE stems from their incompletely filled f-shells, whose inner charge distribution make them less sensitive to the electronic environment. Thus, despite the low absorption coefficients caused by parity selection rules, the PL resulting from *4f-4f* transitions has been frequently used because of the narrow and defined lineshapes in the NIR region. On the other hand, *4f-5d* transitions fall in the visible range, thereby altogether providing a platform for down-conversion.

The RE doping of LHPs thin films and NCs has been the subject of intense investigations in the last few years.[142,177–183] Song et al. reported the doping of $CsPbCl_3$ NCs using different RE cations (Ce^{3+}, Sm^{3+}, Eu^{3+}, Tb^{3+}, Dy^{3+}, Er^{3+}, and Yb^{3+}).[183] Differently from the Mn^{2+} ion, RE ions were demonstrated to stabilize the tetragonal form of $CsPbCl_3$, as confirmed by the strong (101) XRD peak. Again the structural effect was caused by the lattice contraction following the replacement of Pb^{2+}

with the smaller Ln^{3+} cations. On the other hand, analogous to what was reported for Mn^{2+}, the PL spectra exhibited not only the NCs exciton emission peak but also many other narrow emission bands associated with the dopants (Figure 8c). These emissions were assigned to the *5d-4f* transitions of the Ln^{3+} ions sensitized by the host NCs, as confirmed by the matching of their PLE with the NCs absorption.

Notably, the doping resulted in increased PLQY of the NCs exciton band, and prolonged emission decays (from $\tau_{NC} = 4.1$ ns up to $\tau_{Yb:NC} = 9.1$ ns), therefore suggesting that dopant ions increase the defect passivation. Bakr et al. further explored this concept achieving a giant photoluminescence enhancement from 1 to 60%, by treating $CsPbCl_3$ NCs with YCl_3. Y^{3+} and Cl^- ions were demonstrated to contribute to passivating Pb-Cl vacancies, thereby decreasing the density of midgap states. Notably, this effect was collaborative by both ion and counterion.[184]

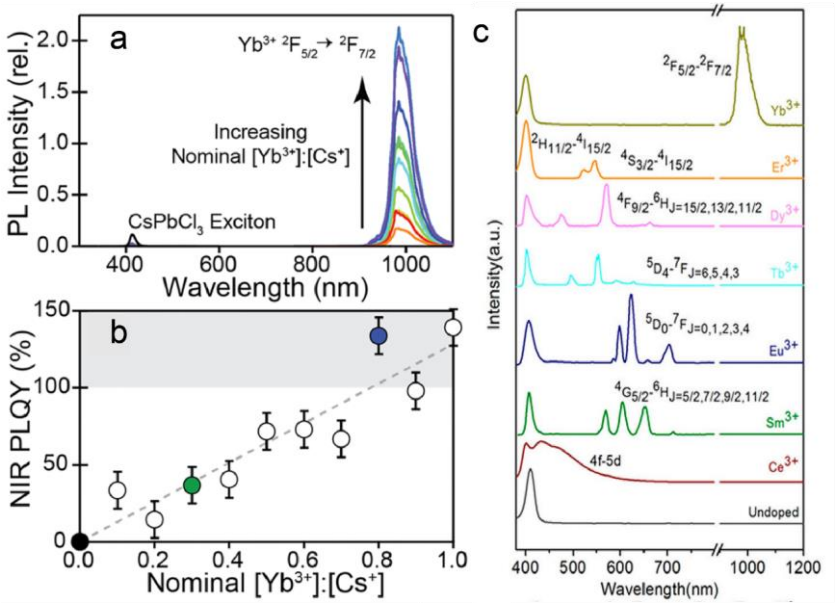

Figure 8. (a) PL intensity and (b) PL quantum yield as a function of increasing Yb concentration in $CsPbCl_3$ NCs. Reprinted with permission from Ref. [179]. Copyright American Chemical Society 2018 (c). Reprinted with permission from Ref. [183]. Copyright American Chemical Society 2017

Among different lanthanides, Yb^{3+} ion doping has aroused the most considerable interest due to its impressive luminescence enhancement, leading to PLQY largely overcoming the unity. The so-called *quantum cutting* process has been demonstrated to underlie this huge efficiency increase.[179,181,182] As shown in Figure 6, this process can generate multiple excitons through the absorption of one single high energy photon, similarly to multiple exciton generation in LHPs NCs and singlet fission in organic materials. Gamelin and Song groups systematically investigated this effect in Yb:$CsPb(Br_xCl_{1-x})_3$ NCs.[179,183]

Different from other above mentioned Ln^{3+} ions, the ytterbium ion emission spectrum is dominated by $^2F_{5/2} \rightarrow {}^2F_{7/2}$, a *4f-4f* transition at 988 nm (Figure 8a). Gamelin demonstrated that even low doping concentration ($[Yb^{3+}]$ = 0.7 %), resulted in the complete quenching of the LHP NCs exciton emission (see Figure 8a).[179] Conversely, as shown in Figure 8b, the PLQY of dopant emission shown a constant increase, reaching up to 130% for $[Yb^{3+}]$ = 7.4 %. Temperature-dependent PL studies suggested the presence of thermally-assisted components in the sensitization mechanism.[181] Differently from Mn^{2+}, the Yb^{3+} has a lower degree of covalency with the surrounding lattice, and hence a poorer electronic coupling, which would suggest a slower transfer. According to TA results, that indicate a transfer taking place on a sub-picosecond timescale, Gamelin and co-workers proposed a defect-mediated transfer mechanism. They suggested that the aliovalency of Yb^{3+} plays a role in promoting the quantum cutting process. Indeed, the presence of aliovalent cations induces the formation of charge-compensating defects, assembling into neutral Yb^{3+}-V_{Pb}-Yb^{3+} complexes, akin to McPherson pairs.[180] Hence, the defects complex could rapidly trap LHP NCs excitons and transfer the energy to two Yb^{3+} ions, by exciting them into their $^2F_{5/2}$ excited state, thereby causing the quantum cutting. Noteworthy, the near-matching of this wavelength with the onset of Si PV allowed realizing quantum cutting luminescence solar concentrator (QC-LSC) with record efficiencies. Nevertheless, some inherent limitation of QC-LSC based on Yb^{3+}, i.e., the long PL lifetimes ($\sim$2 ms), leading to saturation under continuous illumination, and the limited stability of $CsPb(Br_xCl_{1-x})_3$, are still major challenges for their actual implementation.[182]

2.4.3 Electrical characterization of endogenously-modified LHPs

Electrical characterization is a useful tool to investigate the physics of the semiconducting LHPs, but an intimate physical contact between the electrode probes and the material is strictly required, even if this might also largely affect the electrical behavior of the sample under examination.[144] Two different structures are used to run electrical measurements, namely the interdigitated [185] and vertical ones.

An interdigitated structure makes use of finger-like patterned electrodes typical of thin-film transistors. This structure is far from the ideal condition of a uniform electric field within the sample due to the dominant edge effects and variable penetration depth, both depending on the electrodes pattern. Besides, it requires insulating substrates (quartz, glass, etc.) to avoid undesired transistor-like polarizations induced into the substrate by capacitive coupling or applied bias.

On the other hand, large area top and bottom electrodes sandwiching the material under examination make a vertical structure, traditionally called metal-insulator-metal (MIM) structure.[143,144] Assuming a square structure for electrodes, the large areas imply that the material thickness is orders of magnitude lower than the side of the square electrodes, thus getting as close as possible to the ideal structure of a capacitor with parallel plates. When this condition is satisfied, it is possible to assume a uniformly distributed electric field on the surface of the electrodes that largely simplifies the modeling of such a device. Despite looking simpler, the vertical structure is much harder to realize due to processing issues.[186] While the creation of the bottom contact may be trivial, the deposition of a compact active-layer (the material under test) often requires a lot of tuning and optimization, since it must be pinhole-free to avoid shunting between the two electrodes. A further issue arises with the top contact, since it needs to adhere correctly to the (usually) rough surface of the studied material. However, when adequately built, the vertical MIM is the best structure for semiconductors characterization, due to its closeness to the ideal conditions hypothesized during modeling. Furthermore, for the specific case of LHP, the vertical structure better approximates the final device structure of a PV device. Focusing on the electrical characterization of doped/defect engineered

materials, several works usually adopt interdigitated structures for preliminary studies, followed by vertical structure for modeling purposes.

Among the most common electrical characterization for defects analysis and doping effects, the thermal admittance spectroscopy (TAS)[175,187], impedance spectroscopy (IS),[188,189] capacitance-voltage (C-V)[190,191], deep level transient spectroscopy (DLTS)[192,193], transient voltage decay, transient current decay, open-circuit voltage decay (OCVD),[194,195] charge extraction (CE), transient photo-voltage (TPV), transient photo-current (TPC) and current density-voltage (J-V) techniques are the most informative.

TAS is a powerful AC technique, particularly useful on low-doped or high resistivity semiconductor to detect the activation energy of trap states. This technique measures the capacitance or admittance of a semiconductor over a range of frequencies and temperature identifying the activation energy threshold at which the traps within the semiconductor release or capture charges, as shown in Fig. 9a. Typically, in TAS, each step in capacitance or peak in admittance corresponds to a different threshold in frequency or temperature, which plotted in an Arrhenius plot give the activation energy of the defects under investigation.[187]

DLTS is a transient technique exploiting the change in capacitance or current throughout a non-equilibrium state at different temperatures, to extrapolate the energy capture and capture cross-section of defects. Suitable for highly doped semiconductors, it is particularly interesting to investigate the effect of charge trapping/de-trapping within charge depletion regions.[193]

C-V data of a diode-like structure allow the estimation of the doping concentration and distribution in standard inorganic semiconductors.[196] While its validity on silicon devices has been comprehensively proved and studied, its usage with organic and hybrid semiconductors is still under debate, despite being widely applied.[197]

IS tests the J-V frequency response of a device under different steady-state bias conditions (temperature, illumination, voltage/current) on a wide frequency range, which usually spans from

μHz to MHz. IS, in combination with modeling, provides a powerful tool to characterize material and interface properties, including the charge transport and recombination.[198]

OCVD[199], TPC, TPV, as well as transient current/voltage decay techniques exploit the transient phenomena occurring after a change in bias conditions (i.e., light, voltage, or current). Depending on the measurement type and the bias starting/ending points, by using proper modeling these techniques allow extracting parameters like (minority) charge density and transport/recombination time constant.[194]

J-V (4-probe) is the simplest among the electrical characterization techniques and is usually underestimated. Indeed, advanced J-V data processing and modeling allow defect and parameter evaluation, as summarized by Rose,[200] which in parallel with other techniques might cast doubts or confirm research results and hypothesis.

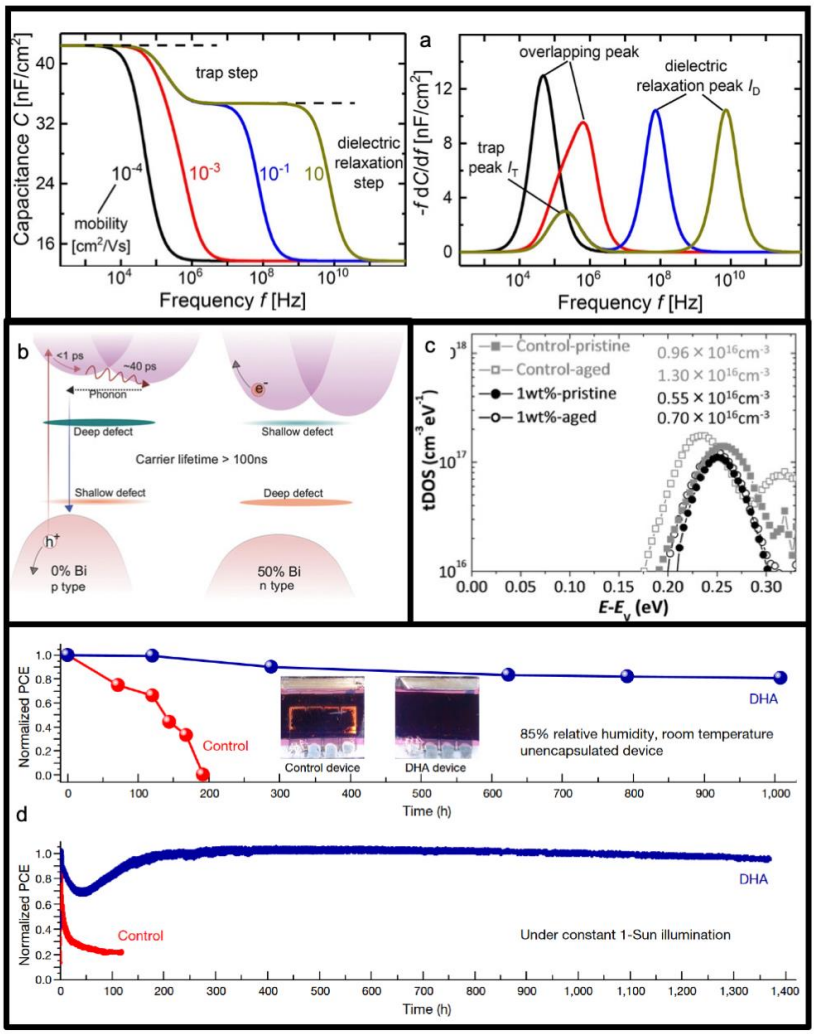

Figure 9. a) Simulated capacitance as a function of frequency (left) and the derived differential capacitance spectra (right). The transitions of the trap peak and dielectric relaxation peak as a function of carrier mobility. The characteristic peaks in the differential capacitance spectra (right) correspond to the capacitance steps (left). I_D and I_T represent the magnitudes of the dielectric relaxation peaks and trap peaks, respectively. Reprinted with permission from ref [187]. Copyright 2018 American Chemical Society. b) Schematic showing the relaxation of carriers to the band edge followed by recombination and the changes in defect levels on cation transmutation. Reprinted with permission from ref [175]. Copyright 2018 John Wiley and Sons. c) Defect energy distribution within complete PSC with neat (control) and 1 wt% N-DPBI doped C_{60}

electron-transporting layers (1 wt%) both before (pristine) and after aging (aged) for 25 d in a dry desiccator in the air without encapsulation. Reprinted with permission from ref [201]. Copyright 2018 John Wiley and Sons. d) Results of humidity stability tests on the unsealed (top) encapsulated (bottom) controls and double-layered halide architecture (DHA) devices under 85% relative humidity at room temperature (top) or 1-Sun illumination (bottom). Inset shows photographs of the control (left) and the DHA (right) device after 200 h under 85% relative humidity at room temperature. Reprinted with permission from ref [191]. Copyright 2019 Springer Nature.

Harikesh et al.[175] studied the effects of different metal cations transmutation on lead-free PVK by exploiting electrical characterizations as TAS, AC hall measurements, J-V and TPV. They used 2D layered antimony PVK as the parent compound, replacing the Sb cation with an isoelectric heavier Bi cation at different percentage $(NH_4)_3(Sb_{(1-x)}Bi_x)_2I_9$ (x from 0 up to 0.5) which affects the PVK conductive properties, switching the intrinsic *p*-type lead-free PVK into an *n*-type one. They used a vertical structure (TiO_2/lead-free PVK/(Poly(4-butyl phenyl diphenylamine))/Au) to run TAS and C-V, while they exploited an interdigitated structure to study the PVK switchable photovoltaic effect, previously evidenced by Xiao et al.,[202] on this specific lead-free PVK material with different Bi percentages. DFT simulation and optical-electrical experimental measurements point to the same results. Progressive Bi substitution shifts the CB and the VB downward while maintaining the same direct/indirect gap properties. However, since the material has fixed (or slightly affected) defects in the bandgap, its semiconducting behavior changes from *p*-type to *n*-type with the shifting of the CB and VB, as shown in Fig. 9b. The AC hall-effect measurement (i.e., an essential technique to detect the charge carrier type and mobility) confirms simulations, while the TAS measurements provide CB and VB shift with increasing Bi concentration. TAS proved indeed that the location of the defect relative to CB and VB changes with increasing doping and the authors suggested that this is due to the different ion weight (compared to Sn) that shifts the PVK bands downward. However, further research is necessary to define the limits of TAS in defects analysis, as explained by Wang et al. in their work.[187] Harikesh et al. work represents an extensive investigation, fully comprehensive of all the necessary measurements to gain complete knowledge of the material´s electrical properties.

Some of the authors [133] conducted a correlated study on the effects of ion migration within MAPI NCs obtained through laser-ablation from a target precursor and deposited on interdigitated devices. In this work, we investigated the effect of long-term polarization on the performance of MAPI, by analyzing current injection and extraction into/from the LHP film. We proved that the high electric field generated at the interfaces with the electrodes due to migrating ions is disruptive for the LHP film lattice since during the long steady-state characterization it degenerates the MAPI into its precursors (MAI and PbI_2), the hypothesis is also supported by Raman measurements.

Son et al.[203] showed the possibilities offered by doping LHPs (specifically, MAPI, $FAPbI_3$, $FA_{0.85}MA_{0.15}PbI_{2.55}Br_{0.45}$ and $FA_{0.85}MA_{0.1}Cs_{0.05}PbI_{2.7}Br_{0.3}$) with alkali iodides (LiI, NaI, KI, RbI and CsI). Defects engineering within LHPs and reduction of electrical hysteresis was the aim of their work, lowering the number of trap states generated by defects. KI stem as the most successful dopant in reducing hysteresis. They used MIM devices and complete PSCs in order to study the effects of doping on PV performances by J-V and IS measurements, in parallel with DFT calculations.

By analyzing IS data on MIMs and PSCs, they stated that both structures have a similar behavior and defects identity must necessarily be that of bulk defects. By modelling J-V in dark with space-charge-limited (SCL) current model and exploiting the dielectric constant from IS data, they extrapolated the trap density (n_t) within the bulk material.[200] n_t indeed decreases by increasing KI doping, at least below a certain level of doping.

The authors, based on DFT simulations, have also discussed the reduction of hysteresis potential upon K-doping. According to them, the incorporation of K occurs mainly in interstitial position within the lattice. The saturation of interstitials sites induced by alkali-doping increases the energy of formation and reduces the mobility of the iodine Frenkel defects, responsible of the J-V hysteresis. Other works explored the advantages of doping the layers in close contact with LHP and studied the effects on the resulting interfaces. Indeed, while the doped material is that of the transporting layers, the intimate contact of these ancillary layers with LHP usually affects the LHP defects distribution at the interface. In this regard, Wang et al.[201] doped the C_{60} electron transport layer (ETL) with N-DPBI and tested

this ETL in an n-i-p PSC. They run TAS on the PSCs built with the doped-ETL at different percentage and the resulting density of states (DOS) proved that doping helps in improving the stability of the PSC, despite an increased wettability. Indeed, the DOS of the LHP does not change with aging while it does with a neat C_{60} ETL, as shown in Fig. 9c. Wang et al. therefore, disclosed some interesting results on the possibilities offered by doping the layers directly interacting with the LHP absorber, which may lead to interfacial doping of the LHP material itself, improving stability and reliability of PV devices.

Moving towards the anode side, Jung et al.[191] successfully improved the LHP/hole transport material (HTM) interface by treating the surface of the LHP prior to HTM deposition with n-hexyl trimethyl ammonium bromide. The treatment created a thin layer of wide-bandgap halide (WBH) LHP on top of the narrow bulk absorbing layer, which granted high performance even by using the low-cost poly(3-heylthiophene) (P3HT) as HTM that can, in principle, overcome the limitations usually encountered by researchers when developing PSC with SPIRO-OMeTAD molecule.[204] J-V, C-V and maximum power point (MPP) electrical characterizations proved enhanced performance, as shows MPP tracking in Fig. 9d.

Regarding transient electrical measurements, Walter et al.[194] approached the study of transients in LHPs by numerical simulation of the measured photo-voltage behaviors. Walter et al. model includes non-radiative recombination and drift-diffusion of both ions and hole/electrons within LHPs, reaching good qualitative results. However, further research and tuning of this model is necessary in order to extrapolate reliable physics quantities, such as the ion density, mobility and diffusion constant, before this approach allows quantifying the effects of doping/defect engineering efficaciously.

Finally, as a reference case of the possibilities given by electrical characterizations to assess the performance of an LHP material, the work of Zhang et al.[205] deserves to be summarized here. These authors indeed reported the results of post-device ligand (PDL) treatment on fabricated PSCs. Exploiting both common steady-state and modulated measurements, they showed that the application

of diethylenetriamine (DETA) as room-temperature PDL treatment to fully processed PSCs highly improves solar cells stability and performance. The authors suggested that the main reason behind these improvements is the repairing and healing of defects in the PVK active region, which enhances performances by reducing non-radiative charge recombination. MPP tracking, J-V, IS, and light dependence of V_{OC} in the studied devices were monitored throughout the experiment, in parallel with XRD, UV-vis absorption, SEM, XPS, and TRPL for physicochemical characterizations. The synergy of these several characterizations allowed the validation of the authors' hypothesis and reinforced the idea that only by deep investigation and multiple technique comparison it is possible to get a broader view of the issues behind observed phenomena.

3. Exogenous strategies

Compositional engineering, *i.e.*, the chemical doping processes discussed previously in details, is at the focus of the widest amount of work carried out by researchers all over the world to improve the quality of LHP materials for the optimization of real devices optoelectronic properties.

However, in the last four years, several manuscripts have been published concerning the use of LHPs in many fields, including energy harvesting, LEDs, photodetectors, sensing and photocatalysis, in combination with other organic or inorganic frameworks as nano-composites, aiming at realizing brand new material platforms capable of solving specific technological problems. These efforts for "coupling" LHPs with materials having complementary properties or able to boost LHP native ones are at the base of the constantly increasing uses of LHPs beyond the sole PV field.

Thus, this final section of the review is devoted to summarizing and analyzing critically those research results dealing with the emerging area of LHP-based nano-composites.

1.1. LHP-based polymer nanocomposites for optoelectronics

The combination of LHPs with polymers has emerged as a valuable strategy to target technological applications of these nanomaterials going beyond the classical use in PV. LHP-based polymer composites are a strategical platform to exploit the properties of the two different components towards

specific targets, in a cooperative fashion that allows the strengthening of each material's native properties or the interplay between individual characteristics.[206]

The use of polymers as additives/templates to control LHP film morphologies[207] emerged around 2014, with different examples aiming at the construction of PSC with improved PCE.[208–211] Colella and coworkers conducted fundamental studies on the interactions occurring between prototype polymers, both classical and conjugated ones, and MAPI precursors, looking for a general protocol to control the size and shape of the aggregates that form initially in solution and then being able to address film morphology.[212] Specifically, through a combination of NMR spectroscopy, dynamic light scattering and microscopy techniques, they found that a higher number of hydrogen-bond interactions between protons on MA^+ and oxygen/nitrogen-rich sites on the polymer chains determines the formation of smooth LHP:polymer films. On the other hand, the lack of these specific sites for non-covalent interactions favors the formation of micron-size MAPI aggregates in solution, that ultimately give rise to bundles-containing films (see Figure 10a for a pictorial representation of this concept). The same group in 2018 made use of the knowledge previously obtained to build environmentally friendly LHP:polymer films, to obtain 17.2% PCE in a fully solution-processed planar PSC stable to high-moisture contents (50%) and resistant to bending stress.[213] The selected macromolecule was this time a starch biopolymer that, with its abundance of oxygen sites suitable for hydrogen bonding with MA^+, positively influenced the formation of continuous PVK films via single-step coating. This was made possible by the occurrence of a gel-like behavior in the starch:PVK precursor composite solution (Figure 10b). Again in 2018, these authors further extended the concept of exploiting hydrogen bond interactions to influence the self-assembly process leading to highly crystalline MAPI films for PSCs by employing cyclodextrins as templating agents, which are thermally removed/decomposed during the annealing process.[214] Even if not properly based on an LHP:polymer composite, this approach deserves to be nominated here because of its great potential for the development of tailored composite materials.

Commentato [TG5]: add ref:
https://doi.org/10.1016/j.nanoso.2017.02.001
has nothing to do with the review, but rev 1 asksfor it

Commentato [TG6]: add ref:
https://doi.org/10.1016/j.nanoso.2017.09.017
no sense, but wanted by rev 1

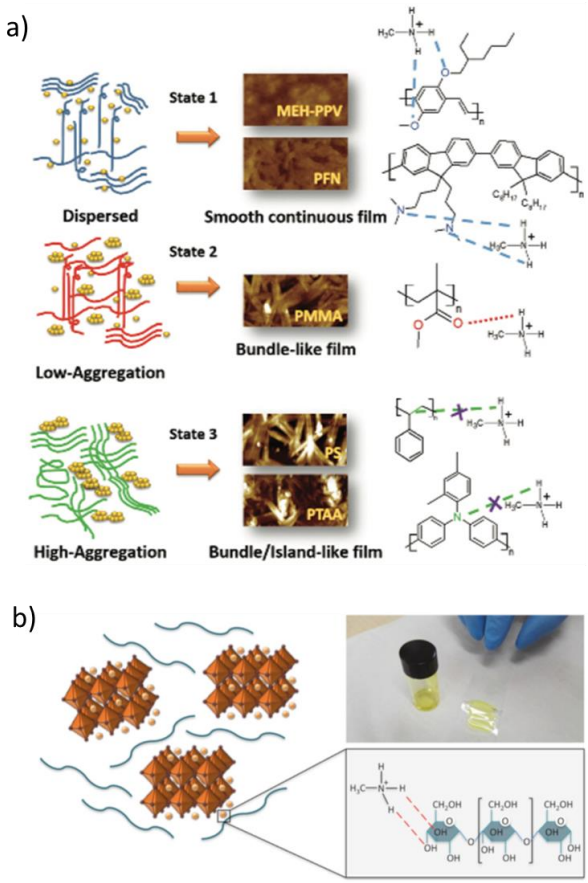

Figure 10. a) Schematic representation of the selective hydrogen-bond interactions taking place between MA^+ in the MAPI precursors and oxygen/nitrogen rich sites on the polymer backbones, investigated by Colella and coworkers. The relationships with the resulting film morphologies are also schematized, highlighting how a lower amount of these interactions in the composite precursor solution induces the formation of bigger aggregates and, consequently, inhomogeneous films. Reproduced from ref [212] with permission of the Royal Society of Chemistry. b) Formation of a gel-like MAPI:starch biopolymer precursor (photo) and detail on intermolecular interactions established within it. Adapted from ref [213] with permission of Elsevier.

Many authors have pursued the incorporation of LHP-NCs/QDs into polymer matrices to improve processability, film quality, and stability of these nanomaterials in the last 3 years.

With the specific aim of enhancing the PL/electroluminescence (EL) properties of the LHP-NCs, Zhong and coworkers in 2016 resorted to the fabrication of films of $MAPbBr_3$ NCs embedded into a polyvinylidene fluoride (PVDF) phase, having outstanding thermal, mechanical, hydrophobic and film-forming properties, in conjunction with the well-known piezoelectricity (vide infra for discussion on flexible LHP:PVDF piezoelectric generators).[215] Starting from a single DMF solution containing both the $MAPbBr_3$ NC precursors and PVDF, the use of a two-step solvent evaporation process (first in vacuum and then through heating in an oven) allowed the separation of the LHP and PVDF crystallization process, providing bright green emissive films with good transparency in the 540-900 nm region. The green composite films were employed in a white LED structure in combination with a blue and a red layer, providing a device with high luminous efficiency (up to 109 lm W^{-1} at 20 mA current).

The group of Alivisatos also reported back in 2016 the encapsulation of $CsPbBr_3$ QDs in a high molecular weight hydrophobic triblock copolymer of polystyrene (PS) and studied systematically the retention of the PL in films of this composites kept under water-soaking conditions.[216] The protective effect of the polymer was significant: 3 μm spun-cast films of the composite were able to retain a stable PLQY after four months of complete immersion in water, differently from what happened with a film of the sole $CsPbBr_3$ QDs lacking any protection (see Figure 11a). Wei et al. applied a simple swelling-shrinking strategy in non-polar solvents to produce luminescent $CsPbX_3$@PS (X = Cl, Br, I) composite beads with superior resistance to water.[217] Interestingly, the beads were also very stable in biological media, not releasing any toxic Pb^{2+}. Cells seeded in their presence incorporated the luminescent composites within the external membrane, foreseeing for these nanomaterials an interesting future use as efficient luminescent probes for cell membrane labeling. A further step into LHP-NCs/QDs stabilization towards the action of protic solvents such as water or methanol, further accompanied by enhanced thermal stability, was reported by Liu and coworkers through the production of ternary graphene oxide (GO)-polymer-$CsPbX_3$ composites able to self-assemble into nanorod-like superstructures.[218] The $CsPbX_3$ NCs were directly grown *in situ* on a

poly(acrylic acid)-grafted GO (GO-g-PAA) binary composite as shown in Figure 11b, thanks to the coordinating action of the PbX_2 precursor on the carboxylate residues pending from the polymer chains, forming convenient nucleation sites for NCs formation. The induction of the nanorod-shaped suprastructures was achieved by treating the colloidal solution of the ternary composite in toluene with hexane. HR-TEM analysis highlights how the LHP-NCs are well-embedded within the nanorods (Figure 11c) and thus perfectly encapsulated. The protective action of these hierarchical structures was evaluated once again by measuring the residual PLQY of the samples in methanol and water after different times. In both cases excellent PL intensity retentions were found, paving the way to the potential use of these materials in photocatalysis, considering the presence of GO, which can improve charge separation and transport.

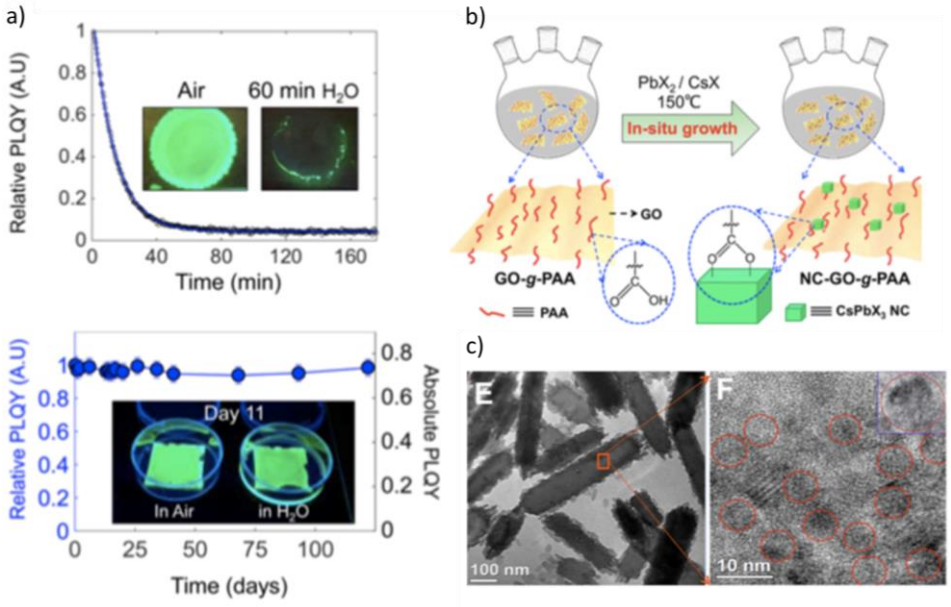

Figure 11. a) Trends in PLQY over prolonged ageing times for the $CsPbBr_3$ QDs (top) and $CsPbX_3$@PS (bottom) in both air and water studied by the group of Alivisatos. b) Pictorial representation of the synthetic process employed by Liu and coworkers to produce ternary $CsPbX_3$-NC-GO-g-PAA composites, with specific focus on the *in situ* growth of the LHP-NCs. c) HR-TEM images of the nanorod-like superstructures formed by the ternary $CsPbX_3$-NC-GO-g-PAA composites

and detail on the LHP-NCs, appearing well-encapsulated within the hierarchical structure of the binary GO-g-PAA matrix. Reproduced from ref [216] and ref [218] with permission of the American Chemical Society.

An interesting approach for the fabrication of $CsPbBr_3$ NCs/poly(methyl)methacrylate (PMMA) composites in the form of nanofibers was reported by Ma et al. employing a microfluidic spinning technique.[219] More precisely, the method allowed first to build 1D/2D microreactors, which were used for the large-scale continuous production of the $CsPbBr_3$/PMMA composites without the simultaneous generation of toxic solvent waste containing heavy metal ions. In an attempt to integrate the formation of LHP NCs and of the polymer guest matrix in a one-pot reaction, Xin et al. developed a general strategy for the production of LHP NCs@polymer composites that can be applied to many commercially available monomers undergoing thermal or UV polymerization in the presence of a suitable initiator.[220] The method involves the use of only a trace amount of DMF to dissolve the PVK precursors and it is therefore a green technique, with excellent perspectives for industrialization. By controlling the loading content of PVK NCs in the polymer phase, it is possible to act beneficially in reducing NCs self-aggregation, generally leading to undesired PL quenching. In addition, the concomitant production of the polymer chains and of the NCs prevents possible post-production phase separation phenomena, which are common in composites obtained through simple blending approaches of pre-formed components, due to the large discrepancy in polarity between PVK and polymers. Highly water resistant $CsPbBr_3$@PMMA polymer nanospheres were reported by Li and coworkers, employing a spray-assisted coil to globule transition method for the efficient encapsulation of the LHP QDs inside the polymer phase.[221] The robust coverage with PMMA limited almost completely the toxicity of the $CsPbBr_3$ QDs, allowing the use of the composite nanospheres (with 110 nm average diameters in water) in live-cell imaging.

The production of LHP@polymer composites is not only useful to provide robustness to LHP NCs or QDs but can also represent a very practical material platform to target different energy-related,

optoelectronic, and sensing applications. We will now discuss examples from the recent literature of LHP@polymer composites used in LED, lasing, piezoelectrics, sensors, and photodetectors.

The first example of an LED based on a LHP@polymer composite was reported in 2015 by Yu and coworkers, employing $MAPbBr_3$ and poly(ethylene oxide) (PEO).[222] The morphology of the composite films was controlled by changing the weight ratio between the PVK precursors and the polymer, thus evidencing the decrease in LHP crystal sizes with the increase in PEO content, together with the improvement in film homogeneity, becoming smooth and pinhole-free (see Figure 12a). The 1:0.75 LHP:PEO ratio was found to be the optimal one for the green LEDs fabrication, providing a device with low turn-on voltage (2.9 V) and high brightness (4064 cd m^{-2} at 5.5 V). In a later contribution (2017), the same group reported a stretchable version of the same PVK-based green LED, employing the LHP@PEO composite in the emissive layer and a PEDOT:PSS/PEO mixture as the hole injecting layer.[223] The device was demonstrated to be reversibly stretchable up to 40% strain for 100 cycles, continuing to emit a uniform green light (Figure 12b). The combination of $FAPbBr_3$ with PEO allowed Chen and coworkers to build also a two-photon-pumped random laser.[224] This type of devices can represent a good solution for low-cost thin-film lasing technologies for flexible speckle-free imaging and projection application.

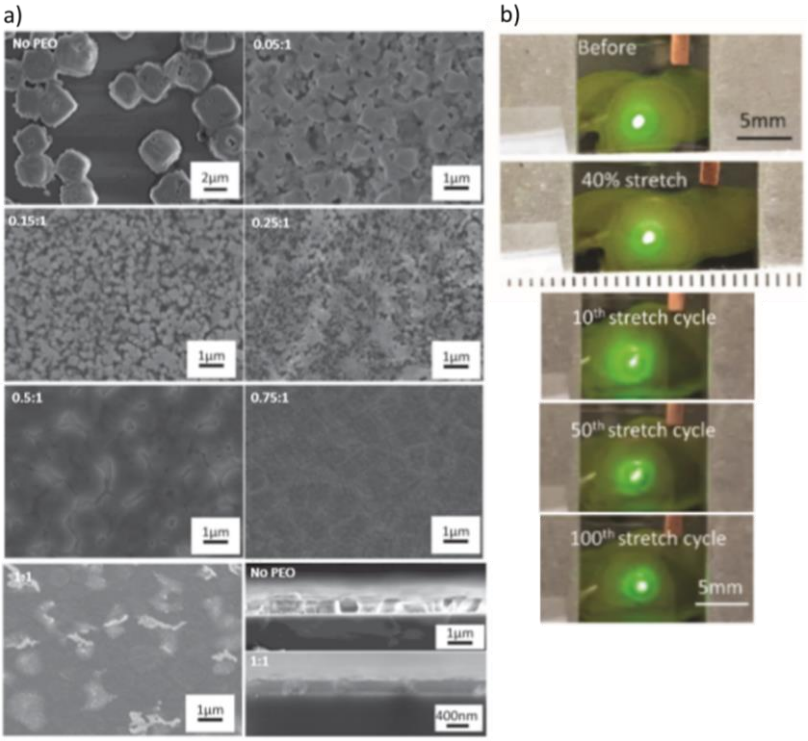

Figure 12. a) Evolution in LHP film morphologies observed through scanning electron microscopy after the addition of increasing amounts of PEO. b) The visual appearance of a green LED based on a LHP@PEO light emitting layer before (top) and after (center) stretching to 40% strain and after 10, 50 and 100 stretching cycles at 0-40% strain (bottom). Adapted from refs [222] and [223] with permission of Wiley.

Yang and coworkers reported on the fabrication of a pure white LED (CIE coordinate at 0.33,0.34) by combining blue-emitting PVK nanocrystals and an orange semiconducting polymer, namely the well-known poly[2-methoxy-5-(2-ethylhexyloxy)-1,4-phenylenevinylene] (MEH:PPV).[225] More recently, Lin et al. produced with electrospinning stretchable membranes of highly hydrophobic (poly(styrene-butadiene-styrene) (SBS) nanofibers embedding $CsPbX_3$ NCs (X = Cl, Br, I) (Figure 13).[226] These composite fibrous materials are stable to water damage, with unvaried PL values after 1 hr of total immersion. An optimized white LED was obtained by employing red and green

LHP NCs@SBS nanofibers on a blue-chip, emitting a warm white light with a luminous efficacy of up to 9 lm W^{-1} and a broad color gamut.

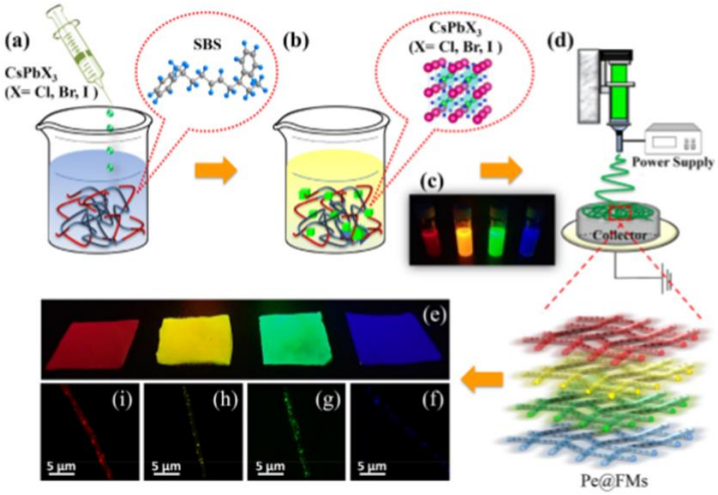

Figure 13. LHP NCs@SBS electrospun nanofibers produced by Lin et al. with different emissive behavior based on the embedded LHP NCs. Reproduced from ref [226] with permission of the American Chemical Society.

As mentioned previously, composites of PVK and PVDF are attracting considerable attention for the construction of flexible piezoelectric generators able to scavenge energy from the environment and biomechanical movements. A comprehensive review on the use of PVK in these devices has been recently published, to which we refer for details.[9] Here we will only briefly treat two cases of polymer composites, that are the exact subjects of this review. In 2017, Ding et al. described an efficient piezoelectric generator based on $FAPbBr_3$ NCs dispersed in PVDF, mainly benefiting from the piezoelectric properties of both the material constituents.[227] The $FAPbBr_3$ NCs are indeed characterized by remarkable ferroelectric properties, with a high piezoelectric charge coefficient of 25 pm V^{-1}. At the same time, also PVDF, in its β phase is characterized by good piezoelectricity, with a coefficient of -29 pm V^{-1}. The authors thus achieved a maximum piezoelectric output voltage of 30 V and current density of 6.2 μA cm^{-1} by employing a 12 wt% concentration of $FAPbBr_3$ NCs in PVDF and used the alternating generated output signals to charge a capacitor and light up a red LED (see

Commentato [TG7]: add ref: https://doi.org/10.1016/j.nanoso.2018.12.002 this ref deals with piezo based on pvdf and perov oxide, therefore we add it since requested by rev 1, but do not comment it

Figure 14a). The group of Mandal reported a porous MAPI-incorporating PVDF β phase film through solution casting in air.[228] The dispersion of the MAPI NCs inside the hydrophobic PVDF matrix allows for their protection from moisture and oxygen. On the other hand, the presence of the LHP NCs appeared to be the reason for the induction of the β phase in PVDF and the formation of the porous morphology, with average pores diameters around 550 nm (Figure 14b left-side). The porous composite was demonstrated to be suitable for harvesting biomechanical energy from the human body, by charging different capacitors under continuous dynamic tactile stimuli. Also, the presence of the MAPI-NCs made photoactive such a material platform, extending its potential for the preparation of a self-powered visible light photodetector (see Figure 14b for the device characteristics). A porous composite of $MAPbBr_3$ NCs embedded into a PVDF matrix was also reported very recently by Yu and coworkers for the fabrication of a nanograms-sensitive sensor for explosives belonging to families of compounds such as nitroaromatics, nitroamines and nitrate esters.[229] Pore sizes of 2-10 μm, coupled to wall thicknesses of hundreds of nanometers, were obtained by resorting to a freeze-drying process. A progressive PL quenching in the presence of increasing amounts of organic nitro explosives takes place in the composite and the reason for this behavior is found in an increase in traps density rather than in a photoinduced charge transfer process between the sensor and the analytes.

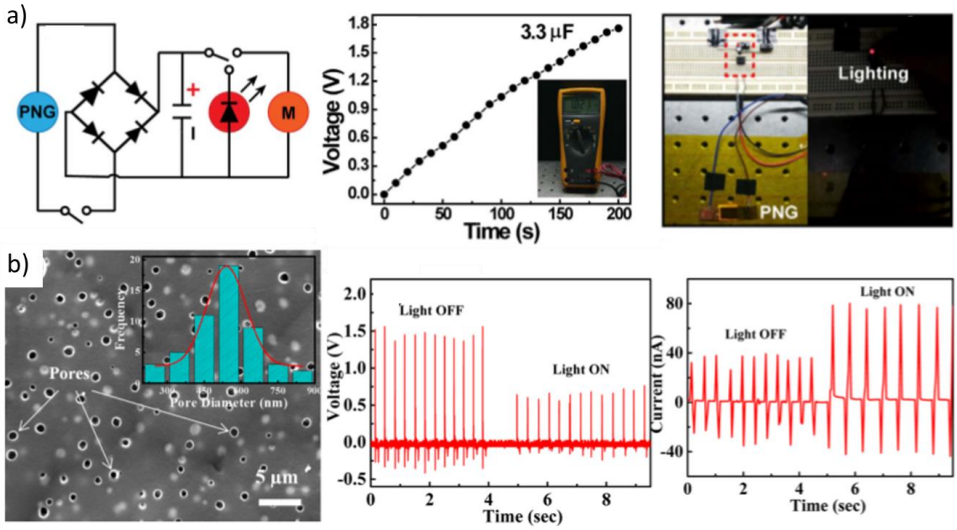

Figure 14. a) Capacitor charging and red LED lit up using the electric energy provided by the periodic pressing of the $FAPbBr_3$ NCs@PVDF based piezoelectric generator reported by Ding et al. Reproduced from ref [227] with permission of Elsevier. b) On the left side, the porous morphology by SEM of the MAPI NCs/PVDF composite prepared by Mandal and coworkers is shown. On the right side, the change in piezoelectric response (output voltage and current) in dark and in light under continuous application and removal of stress of the hybrid piezoelectric/photodector device is reported. Adapted from ref [228] with permission of the American Chemical Society.

The group of Yu fabricated flexible X-ray detectors by employing lead-free $Cs_2AgBiBr_6$ double perovskite crystals dispersed in different polymer matrices.[230] The best results in terms of film homogeneity were obtained when polyvinyl alcohol (PVA) was used as the host matrix, likely because of the polar interactions that it can establish with the PVK through the pendant hydroxyl groups. The devices based on free-standing 100 μm-thick films of the 2:1 $Cs_2AgBiBr_6$:PVA composite exhibited an excellent sensitivity to X-rays, and they could be bent with a 2 mm radius without leading to any photocurrent degradation.

1.2. Combination of LHPs with inorganic materials

LHP-based photodetectors are generally emerging as new promising technologies because they demonstrate outstanding photo-responsivity and detectivity. To enlarge the optical window of these devices towards the NIR region, nanocomposites were realized by Li et al. using solution-processed up-conversion nanoparticles (UCNs) like $NaYF_4$:Yb/Er deposited on a flexible polymeric substrate.[231] In this work, the authors employed MAPI microarrays coupled to the UCNs thin film, exhibiting superior performances with respect to standard LHP-based NIR photodetectors, achieving a maximum responsivity of 0.27 AW^{-1} and detectivity of 0.76 10^{12} Jones, thanks to the efficient energy transfer between the MAPI arrays and UCNs layer (Figure 15a). Similar results were obtained by Wang et al.[232] reporting on a system in which the UCNs are surrounded by MAPBr nanowires, able to achieve a 28.5% efficiency in the energy transfer process and allowing the subsequent realization of a NIR photodetector. A particular example of inorganic LHP-based composite for photodetector is reported in ref [233] where Li and coworkers dipped a carbon fiber covered with TiO_2 in an LHP precursor solution and, by suitable solvent engineering, induced the nucleation of LHP NCs on the surface of the fiber. The system was then twisted with a CuO wire, able to suppress dark current of LHP, realizing a broadband photodetector with high detectivity (about 10^{13} Jones, at least two orders of magnitude better than other reported LHP-based photodetectors).[234]

LHP-based LED suffer from chemical and structural instability that can be reasonably fixed by coupling the PVK cores with inorganic scaffolds, akin to what discussed in the previous paragraph for polymeric ones. Silica shells, for instance, can be exploited for the realization of moisture and heat stable white LEDs. In Zhang and coworkers[235] report, $CsPbBr_3$/silica QDs composites were prepared through a sol-gel reaction using tetramethoxysilane as a precursor. With these species, the authors then realized a stable blue LED, showing 63.5 lm W^{-1} power efficiency, sustained over 13 h of continuous operation in air. Furthermore, phosphosilicate glasses were used instead of silica as an even more robust inorganic barrier against heat-degradation, allowing the realization of devices with tunable emissions in the range 500-750 nm.[236] A 20 lm W^{-1} white LED was realized by coupling the LHP/glass nanocomposite light-emitting systems with a commercial InGaN blue chip. By further

extending the concept, luminescent nanofluids can be used as color converters for LEDs: Lin et al.[237] realized such systems by dispersing LHP NCs in silicon oil and consequently transforming a blue-emitting GaN LED into a green or red-emitting device.

Photocatalysis is another emerging application that may exploit the potential of LHP materials.[238,239] Schünemann et al.[240] developed a direct catalyst for the oxidation of benzyl alcohol to benzaldehyde under visible-light illumination by employing a $CsPbBr_3/TiO_2$ composite through a wet-impregnation method. The composite photocatalyst showed more than 99% selectivity towards the generation of benzaldehyde. Electron spin resonance analysis revealed that the photoexcited electrons in $CsPbBr_3$ transferred to the TiO_2 conduction band are responsible for the concomitant reduction of oxygen, via formation of the superoxide radical. Core@shell $CsPbBr_3$@zeolitic imidazolate nanocomposites were successfully tested for CO_2 reduction.[241] The MOF, directly grown on the surface of LHP QDs, allowed to improve stability to moisture, ability to capture CO_2 and charge separation efficiency (Figure 15b). The electron consumption rate was two times bigger in the case of the core@shell nanocomposite system than in neat LHP QDs[242] and was comparable to that of a $CsPbBr_3$/GO composite system.[243]

Mollick and coworkers also adopted the implementation of MOFs for realizing an ultrastable luminescent nanocomposite for the degradation of organic pollutants in water.[244] Through a pore-encapsulated solvent-directed procedure, $MAPbBr_3$@ZIF-8 (a zeolitic-imidazolate framework) composites were prepared. The MOF walls function as a protecting layer for the PVK core, improving the robustness of the device and allowing the complete degradation in the water of contaminants like methyl orange, methyl red and nitrofurazone (an antibiotic). As discussed already very briefly in the previous paragraph,[218] GO is also useful for triggering photocatalytic properties of LHPs (as well as the long-term stability): in the already cited paper, Xu et al.[243] showed that a $CsPbBr_3$ QDs/GO nanocomposite can convert CO_2 into solar fuels in non-aqueous media under light illumination with a starting reduction rate of 23.7 umol g^{-1} for the neat QDs, which is increased of 25.5% in the nanocomposite, due to the good electron extraction properties.

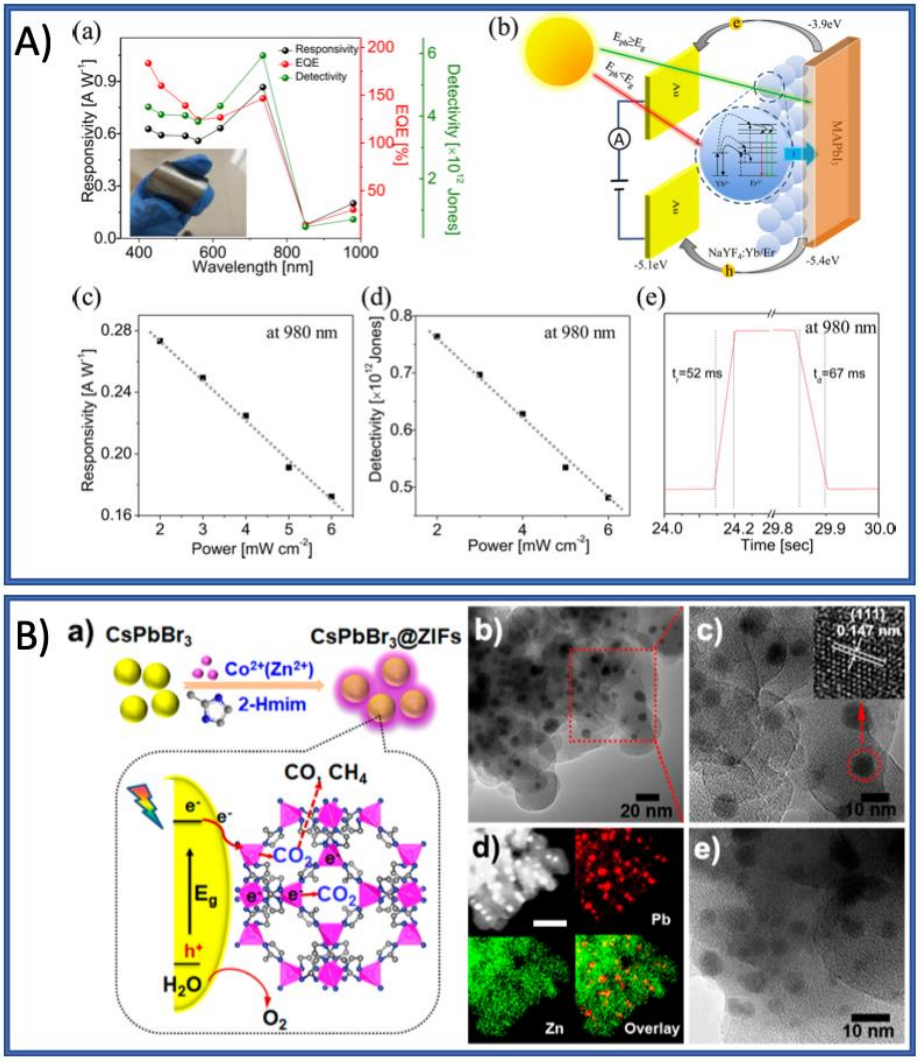

Figure 15. A) a) The highest photoresponse parameters of the bilayer photodetector reported by Li et al. as a function of the incident wavelength. The inset shows the photo of the flexible integrated photodetector. b) Scheme showing the detailed energy transitions from the $NaYF_4$:Yb/Er UCNs to $MAPbI_3$. c) Responsivity R and d) detectivity D* of the bilayer photodetector as a function of NIR irradiance intensity at 980 nm. e) Single photocurrent response cycle with the light switched ON and OFF, showing the response speed of the photodetector at 980 nm. B) a) Schematic illustration of the fabrication and CO_2 photoreduction process of $CsPbBr_3$/ZIFs. b, c) Low- and high- magnification TEM images of $CsPbBr_3$@ZIF-8. The inset of c) is the high-resolution image of a single $CsPbBr_3$ QD marked with a red circle. d) High-angle annular dark-field STEM image and elemental mapping of $CsPbBr_3$@ZIF-8. Scale bar: 50 nm. e) TEM image of

$CsPbBr_3$@ZIF-67. Reprinted with permission from ref.[231] (A) and ref. [241] (B). Copyright 2017 (A) and 2018 (B) American Chemical Society.

4. Conclusions and future perspectives

Albeit five years of intensive research allowed scientists to achieve a good understanding and to harvest many of the low-hanging fruits of doped LHPs, we guess that this field will remain for longer time within the focus of LHP research. Despite the great efforts, effects such as halide segregation in mixed LHP or host lattice-dopant interactions are still to be clarified. These challenges will require the use of innovative approaches, using non-conventional techniques capable of investigating the structure of LHPs in real-time.[245–247] In this contest, the cathode luminescence technique might be useful for investigating the presence of metallic dopants[248], solid-state NMR might become fundamental for quantifying halide segregation within the doped LHP [249,250] and its combination with X-ray absorption for gathering information about long-range lattice order.[251] Also, thermogravimetric analysis can quantify the mass of dopant needed for achieving thermal stability in a PSC,[252] while ultraviolet PL spectroscopy allows for the estimation of Fermi level shifting upon doping.[253]

As a final balance, we can state that PV and other optical applications such as LEDs and photodetectors obtained the most significant benefits from LHP doping, thus being able to reach remarkable optoelectronic performances. However, PV applications suffer from electrical instability given by well-known structural modification issues (ion displacement, grain size modification, defect nucleation and so on) as well as LEDs require stable and consistent emission, i.e., retaining the wavelength emission despite the problem mentioned above.

Indeed, the primary experimental strategy usually applied to provide stability in devices encompasses the use of additives, e.g. small organic molecules, surfactants, ionic liquids, zwitterionic molecules. However, the main setback of this approach is the hampering of the electrical properties and the creation of interface barriers for electrical conduction. On the other hand, we strongly believe that the lattice stabilization induced by LHP doping will be one of the most promising alternatives for

Commentato [TG8]: add ref: https://doi.org/10.1016/j.nanoso.2017.09.001 also no sense citation wanted by rev 1

overcoming these limitations and it will catalyze the efforts of the scientific community in the next years. As evidenced in paragraph 2, the “try and error” approach has been the most applied to reach the present established goals. A reverse approach, based on the design in-silico of new LHPs will likely play a prominent role in the next future. Nowadays, computational techniques based on DFT provide an accurate description of the properties of LHPs at the microscopic level and at reasonable computational costs. Such techniques can be thus applied as screening methods to design effective doping strategies aimed to improve the stability and the performances of LHPs in optoelectronic devices. Furthermore, by exploiting the increasing computer power and algorithms efficiencies, computational modelling opens the possibility to generate large datasets of LHPs structures and properties. The analysis of these datasets by statistical tools based on machine learning will allow to uncover new structure – properties relationships, by opening the way to a data-driven design of novel LHPs with targeted properties.[254,255]

On the other side, in the future, there will be large room for the boosting of those technologies currently not at the focus of LHP scientific community attention, in which the many possibilities of exogenous/endogenous LHP modification will become essential.

For example, thermoelectric LHP-based materials promise to increase the range of PVK energy harvesting applications.[256] Besides the possibilities given by coupling tandem photovoltaic and conventional thermoelectric devices[257,258] exploiting the heat accumulated on the solar cell during operation, theoretical calculations on LHP materials proved that these could work as thermoelectric harvester as well as solar cell,[259] paving the way to a new range of devices optimized both for photons and phonons harvesting.

Furthermore, the photocatalytic applications are extremely promising (through the integration into MOFs or other scaffolds),[11] as well as the fabrication of electrically pumped lasers,[260] the development of LHP-based thermoelectric materials,[256] the realization of highly selective sensors and photo-rechargeable LHP-based batteries.[261] These are only a few examples of applications of LHP that will skyrocket within the next years.

Commentato [TG9]: add these re, which do notmtch ith te topicothe reviw,b ereuesd by re 1:
https://doi.org/10.1016/j.nanoso.2018.05.009
https://doi.org/10.1016/j.nanoso.2016.12.003

One field that will capitalize on the use of LHPs is that of quantum technologies: LHP-based spintronics is gaining a high-interest thanks to the recent discoveries of magneto-optical effects,[262,263] which may in perspective be coupled with the use of magnetic dopants and be used as ultrafast switch or memories. Similar to the progression observed for II-VI QDs, we expect to see a rise in interest for doped-LHP spintronics. Finally, the quest for LHP-based single-photon emitters having a nearly perfect optical coherence has reached its goal with $CsPbBr_3$ NCs, opening to the creation of entangled photon pairs, [264] and future research will expand these results to other pure and mixed halides, and possibly to doped NCs. Lastly, an improved coupling with organic and inorganic materials will also boost the pursuit of strong exciton-photon coupling in LHPs. [DOI: 10.1002/adma.201804894] These advancements will facilitate groundbreaking applications of this such as ultralow-threshold polariton lasers, slowing-light devices and quantum light sources, thereby suggesting that the fields of coherent light sources and polatonic media could be the next big thing for LHPs.

Acknowledgments

T.C.S. and M.R. acknowledge the support from the Ministry of Education AcRF Tier 2 grant MOE2016-T2-1-034 and the NRF Investigatorship NRF-NRFI-2018-04. T.G. acknowledges DFG financial support via the GRK (Research Training Group) 2204 "Substitute Materials for sustainable Energy Technologies".

References

[1] https://www.nrel.gov/pv/assets/pdfs/pv-efficiencies-07-17-2018.pdf. nrel n.d.

[2] Green MA. Third generation photovoltaics: solar cells for 2020 and beyond. Phys E Low-

Dimensional Syst Nanostructures 2002;14:65–70. doi:https://doi.org/10.1016/S1386-9477(02)00361-2.

[3] Meng L, You J, Yang Y. Addressing the stability issue of perovskite solar cells for commercial applications. Nat Commun 2018;9:5265. doi:10.1038/s41467-018-07255-1.

[4] Eperon GE, Hörantner MT, Snaith HJ. Metal halide perovskite tandem and multiple-junction photovoltaics. Nat Rev Chem 2017;1:95.

[5] Leijtens T, Bush KA, Prasanna R, McGehee MD. Opportunities and challenges for tandem solar cells using metal halide perovskite semiconductors. Nat Energy 2018;3:828–38. doi:10.1038/s41560-018-0190-4.

[6] Sutherland BR, Sargent EH. Perovskite photonic sources. Nat Photonics 2016;10:295.

[7] Stranks SD, Snaith HJ. Metal-halide perovskites for photovoltaic and light-emitting devices. Nat Nanotechnol 2015;10:391.

[8] García de Arquer FP, Armin A, Meredith P, Sargent EH. Solution-processed semiconductors for next-generation photodetectors. Nat Rev Mater 2017;2:16100.

[9] Jella V, Ippili S, Eom J-H, Pammi SVN, Jung J-S, Tran V-D, et al. A comprehensive review of flexible piezoelectric generators based on organic-inorganic metal halide perovskites. Nano Energy 2019;57:74–93. doi:10.1016/j.nanoen.2018.12.038.

[10] Wu T, Gao P. Development of perovskite-type materials for thermoelectric application. Materials (Basel) 2018;11. doi:10.3390/ma11060999.

[11] Park G Do, Lee CW, Nam KT. Recent advances and perspectives of halide perovskite photocatalyst. Curr Opin Electrochem 2018;11:98–104. doi:https://doi.org/10.1016/j.coelec.2018.09.009.

[12] Ball JM, Petrozza A. Defects in perovskite-halides and their effects in solar cells. Nat Energy 2016;1:16149.

[13] Goldschmidt VM. Die Gesetze der Krystallochemie. Naturwissenschaften 1926;14:477–85. doi:10.1007/BF01507527.

[14] Li Z, Yang M, Park J-S, Wei S-H, Berry JJ, Zhu K. Stabilizing Perovskite Structures by Tuning Tolerance Factor: Formation of Formamidinium and Cesium Lead Iodide Solid-State Alloys. Chem Mater 2016;28:284–92. doi:10.1021/acs.chemmater.5b04107.

[15] Weber D. CH3NH3PbX3, ein Pb(II)-System mit kubischer Perowskitstruktur. Zeitschrift Fur Naturforsch - Sect B J Chem Sci 1978;33:1443–5. doi:10.1515/znb-1978-1214.

[16] Kim H-S, Lee C-R, Im J-H, Lee K-B, Moehl T, Marchioro A, et al. Lead Iodide Perovskite Sensitized All-Solid-State Submicron Thin Film Mesoscopic Solar Cell with Efficiency Exceeding 9%. Sci Rep 2012;2:591. doi:10.1038/srep00591.

[17] Lee MM, Teuscher J, Miyasaka T, Murakami TN, Snaith HJ. Efficient Hybrid Solar Cells Based on Meso-Superstructured Organometal Halide Perovskites. Science (80-) 2012;338:643–7. doi:10.1126/science.1228604.

[18] Borriello I, Cantele G, Ninno D. Ab initio investigation of hybrid organic-inorganic perovskites based on tin halides. Phys Rev B 2008;77:235214. doi:10.1103/PhysRevB.77.235214.

[19] Eperon GE, Stranks SD, Menelaou C, Johnston MB, Herz LM, Snaith HJ. Formamidinium lead trihalide: a broadly tunable perovskite for efficient planar heterojunction solar cells. Energy Environ Sci 2014;7:982–8. doi:10.1039/C3EE43822H.

[20] Eperon GE, Paternò GM, Sutton RJ, Zampetti A, Haghighirad AA, Cacialli F, et al. Inorganic caesium lead iodide perovskite solar cells. J Mater Chem A 2015;3:19688–95. doi:10.1039/C5TA06398A.

[21] Tenuta E, Zheng C, Rubel O. Thermodynamic origin of instability in hybrid halide perovskites. Sci Rep 2016;6:37654.

[22] Solanki A, Yadav P, Turren-Cruz S-H, Lim SS, Saliba M, Sum TC. Cation influence on carrier dynamics in perovskite solar cells. Nano Energy 2019;58:604–11. doi:https://doi.org/10.1016/j.nanoen.2019.01.060.

[23] Zheng X, Wu C, Jha SK, Li Z, Zhu K, Priya S. Improved Phase Stability of Formamidinium

Lead Triiodide Perovskite by Strain Relaxation. ACS Energy Lett 2016;1:1014–20. doi:10.1021/acsenergylett.6b00457.

[24] Pellet N, Gao P, Gregori G, Yang T-Y, Nazeeruddin MK, Maier J, et al. Mixed-Organic-Cation Perovskite Photovoltaics for Enhanced Solar-Light Harvesting. Angew Chemie Int Ed 2014;53:3151–7. doi:10.1002/anie.201309361.

[25] Tan W, Bowring AR, Meng AC, McGehee MD, McIntyre PC. Thermal Stability of Mixed Cation Metal Halide Perovskites in Air. ACS Appl Mater Interfaces 2018;10:5485–91. doi:10.1021/acsami.7b15263.

[26] Saliba M, Matsui T, Seo J-Y, Domanski K, Correa-Baena J-P, Nazeeruddin MK, et al. Cesium-containing triple cation perovskite solar cells: improved stability, reproducibility and high efficiency. Energy Environ Sci 2016;9:1989–97. doi:10.1039/C5EE03874J.

[27] Saliba M, Matsui T, Domanski K, Seo J-Y, Ummadisingu A, Zakeeruddin SM, et al. Incorporation of rubidium cations into perovskite solar cells improves photovoltaic performance. Science (80-) 2016;354:206 LP – 209. doi:10.1126/science.aah5557.

[28] Ogomi Y, Morita A, Tsukamoto S, Saitho T, Fujikawa N, Shen Q, et al. CH3NH3SnxPb(1–x)I3 Perovskite Solar Cells Covering up to 1060 nm. J Phys Chem Lett 2014;5:1004–11. doi:10.1021/jz5002117.

[29] Park B-W, Philippe B, Zhang X, Rensmo H, Boschloo G, Johansson EMJ. Bismuth Based Hybrid Perovskites A3Bi2I9 (A: Methylammonium or Cesium) for Solar Cell Application. Adv Mater 2015;27:6806–13. doi:10.1002/adma.201501978.

[30] Locardi F, Cirignano M, Baranov D, Dang Z, Prato M, Drago F, et al. Colloidal Synthesis of Double Perovskite Cs2AgInCl6 and Mn-Doped Cs2AgInCl6 Nanocrystals. J Am Chem Soc 2018;140:12989–95. doi:10.1021/jacs.8b07983.

[31] Cortecchia D, Dewi HA, Yin J, Bruno A, Chen S, Baikie T, et al. Lead-Free MA2CuClxBr4–x Hybrid Perovskites. Inorg Chem 2016;55:1044–52. doi:10.1021/acs.inorgchem.5b01896.

[32] Krishnamoorthy T, Ding H, Yan C, Leong WL, Baikie T, Zhang Z, et al. Lead-free

germanium iodide perovskite materials for photovoltaic applications. J Mater Chem A 2015;3:23829–32. doi:10.1039/C5TA05741H.

[33] Noel NK, Stranks SD, Abate A, Wehrenfennig C, Guarnera S, Haghighirad A-A, et al. Lead-free organic–inorganic tin halide perovskites for photovoltaic applications. Energy Environ Sci 2014;7:3061–8. doi:10.1039/C4EE01076K.

[34] Hao F, Stoumpos CC, Cao DH, Chang RPH, Kanatzidis MG. Lead-free solid-state organic–inorganic halide perovskite solar cells. Nat Photonics 2014;8:489.

[35] Akkerman QA, Meggiolaro D, Dang Z, De Angelis F, Manna L. Fluorescent Alloy CsPbxMn1–xI3 Perovskite Nanocrystals with High Structural and Optical Stability. ACS Energy Lett 2017;2:2183–6. doi:10.1021/acsenergylett.7b00707.

[36] Lu M, Zhang X, Zhang Y, Guo J, Shen X, Yu WW, et al. Simultaneous Strontium Doping and Chlorine Surface Passivation Improve Luminescence Intensity and Stability of CsPbI3 Nanocrystals Enabling Efficient Light-Emitting Devices. Adv Mater 2018;30:1804691. doi:10.1002/adma.201804691.

[37] Lamberti F, Litti L, De Bastiani M, Sorrentino R, Gandini M, Meneghetti M, et al. High-Quality, Ligands-Free, Mixed-Halide Perovskite Nanocrystals Inks for Optoelectronic Applications. Adv Energy Mater 2017;7:1601703. doi:10.1002/aenm.201601703.

[38] Zhu C, Niu X, Fu Y, Li N, Hu C, Chen Y, et al. Strain engineering in perovskite solar cells and its impacts on carrier dynamics. Nat Commun 2019;10:815. doi:10.1038/s41467-019-08507-4.

[39] Philippe B, Saliba M, Correa-Baena J-P, Cappel UB, Turren-Cruz S-H, Grätzel M, et al. Chemical Distribution of Multiple Cation (Rb+, Cs+, MA+, and FA+) Perovskite Materials by Photoelectron Spectroscopy. Chem Mater 2017;29:3589–96. doi:10.1021/acs.chemmater.7b00126.

[40] Gratia P, Grancini G, Audinot J-N, Jeanbourquin X, Mosconi E, Zimmermann I, et al. Intrinsic Halide Segregation at Nanometer Scale Determines the High Efficiency of Mixed

Cation/Mixed Halide Perovskite Solar Cells. J Am Chem Soc 2016;138:15821–4. doi:10.1021/jacs.6b10049.

[41] Tress W. Perovskite Solar Cells on the Way to Their Radiative Efficiency Limit – Insights Into a Success Story of High Open-Circuit Voltage and Low Recombination. Adv Energy Mater 2017;7:1602358-n/a. doi:10.1002/aenm.201602358.

[42] Kong W, Ding T, Bi G, Wu H. Optical characterizations of the surface states in hybrid lead-halide perovskites. Phys Chem Chem Phys 2016;18:12626–32. doi:10.1039/C6CP00325G.

[43] Chen S, Wen X, Yun JS, Huang S, Green M, Jeon NJ, et al. Spatial Distribution of Lead Iodide and Local Passivation on Organo-Lead Halide Perovskite. ACS Appl Mater Interfaces 2017;9:6072–8. doi:10.1021/acsami.6b15504.

[44] Minns JL, Zajdel P, Chernyshov D, van Beek W, Green MA. Structure and interstitial iodide migration in hybrid perovskite methylammonium lead iodide. Nat Commun 2017;8:15152. doi:10.1038/ncomms15152 https://www.nature.com/articles/ncomms15152#supplementary-information.

[45] Tian Y, Merdasa A, Unger E, Abdellah M, Zheng K, McKibbin S, et al. Enhanced Organo-Metal Halide Perovskite Photoluminescence from Nanosized Defect-Free Crystallites and Emitting Sites. J Phys Chem Lett 2015;6:4171–7. doi:10.1021/acs.jpclett.5b02033.

[46] Galisteo-López JF, Anaya M, Calvo ME, Míguez H. Environmental Effects on the Photophysics of Organic–Inorganic Halide Perovskites. J Phys Chem Lett 2015;6:2200–5. doi:10.1021/acs.jpclett.5b00785.

[47] Tian Y, Peter M, Unger E, Abdellah M, Zheng K, Pullerits T, et al. Mechanistic insights into perovskite photoluminescence enhancement: light curing with oxygen can boost yield thousandfold. Phys Chem Chem Phys 2015;17:24978–87. doi:10.1039/C5CP04410C.

[48] Stranks SD, Burlakov VM, Leijtens T, Ball JM, Goriely A, Snaith HJ. Recombination Kinetics in Organic-Inorganic Perovskites: Excitons, Free Charge, and Subgap States. Phys Rev Appl 2014;2:34007.

[49] deQuilettes DW, Zhang W, Burlakov VM, Graham DJ, Leijtens T, Osherov A, et al. Photo-induced halide redistribution in organic-inorganic perovskite films. Nat Commun 2016;7:11683. doi:10.1038/ncomms11683.

[50] Lorenzon M, Sortino L, Akkerman Q, Accornero S, Pedrini J, Prato M, et al. Role of Nonradiative Defects and Environmental Oxygen on Exciton Recombination Processes in CsPbBr3 Perovskite Nanocrystals. Nano Lett 2017;17:3844–53. doi:10.1021/acs.nanolett.7b01253.

[51] Motti SG, Gandini M, Barker AJ, Ball JM, Srimath Kandada AR, Petrozza A. Photoinduced Emissive Trap States in Lead Halide Perovskite Semiconductors. ACS Energy Lett 2016;1:726–30. doi:10.1021/acsenergylett.6b00355.

[52] Sadoughi G, Starr DE, Handick E, Stranks SD, Gorgoi M, Wilks RG, et al. Observation and Mediation of the Presence of Metallic Lead in Organic–Inorganic Perovskite Films. ACS Appl Mater Interfaces 2015;7:13440–4. doi:10.1021/acsami.5b02237.

[53] Wang L, Zhou H, Hu J, Huang B, Sun M, Dong B, et al. A Eu³⁺-Eu²⁺ ion redox shuttle imparts operational durability to Pb-I perovskite solar cells. Science (80-) 2019;363:265 LP – 270. doi:10.1126/science.aau5701.

[54] Kim M, Motti SG, Sorrentino R, Petrozza A. Enhanced solar cell stability by hygroscopic polymer passivation of metal halide perovskite thin film. Energy Environ Sci 2018;11:2609–19.

[55] Xu W, Hu Q, Bai S, Bao C, Miao Y, Yuan Z, et al. Rational molecular passivation for high-performance perovskite light-emitting diodes. Nat Photonics 2019. doi:10.1038/s41566-019-0390-x.

[56] Gatti T, Lamberti F, Topolovsek P, Abdu-Aguye M, Sorrentino R, Perino L, et al. Interfacial Morphology Addresses Performance of Perovskite Solar Cells Based on Composite Hole Transporting Materials of Functionalized Reduced Graphene Oxide and P3HT. Sol RRL 2018;2:1800013. doi:doi:10.1002/solr.201800013.

[57] Smith IC, Hoke ET, Solis-Ibarra D, McGehee MD, Karunadasa HI. A Layered Hybrid Perovskite Solar-Cell Absorber with Enhanced Moisture Stability. Angew Chemie Int Ed 2014;53:11232–5. doi:10.1002/anie.201406466.

[58] Mei A, Li X, Liu L, Ku Z, Liu T, Rong Y, et al. A hole-conductor–free, fully printable mesoscopic perovskite solar cell with high stability. Science (80-) 2014;345:295 LP – 298. doi:10.1126/science.1254763.

[59] Van de Walle CG, Neugebauer J. First-principles calculations for defects and impurities: Applications to III-nitrides. J Appl Phys 2004;95:3851–79. doi:doi:http://dx.doi.org/10.1063/1.1682673.

[60] Komsa H-P, Rantala TT, Pasquarello A. Finite-size supercell correction schemes for charged defect calculations. Phys Rev B 2012;86:45112.

[61] Lany S, Zunger A. Assessment of correction methods for the band-gap problem and for finite-size effects in supercell defect calculations: Case studies for ZnO and GaAs. Phys Rev B 2008;78:235104.

[62] Shockley W, Read WT. Statistics of the Recombinations of Holes and Electrons. Phys Rev 1952;87:835–42. doi:10.1103/PhysRev.87.835.

[63] Perdew JP, Burke K, Ernzerhof M. Generalized Gradient Approximation Made Simple. Phys Rev Lett 1996;77:3865–8. doi:10.1103/PhysRevLett.77.3865.

[64] Umari P, Mosconi E, De Angelis F. Relativistic GW calculations on CH3NH3PbI3 and CH3NH3SnI3 Perovskites for Solar Cell Applications. Sci Rep 2014;4:4467.

[65] Filip MR, Giustino F. GW quasiparticle band gap of the hybrid organic-inorganic perovskite CH3NH3PbI3: Effect of spin-orbit interaction, semicore electrons, and self-consistency. Phys Rev B 2014;90:245145. doi:10.1103/PhysRevB.90.245145.

[66] Even J, Pedesseau L, Jancu J-M, Katan C. Importance of Spin–Orbit Coupling in Hybrid Organic/Inorganic Perovskites for Photovoltaic Applications. J Phys Chem Lett 2013;4:2999–3005. doi:10.1021/jz401532q.

[67] Giorgi G, Fujisawa J-I, Segawa H, Yamashita K. Small Photocarrier Effective Masses Featuring Ambipolar Transport in Methylammonium Lead Iodide Perovskite: A Density Functional Analysis. J Phys Chem Lett 2013;4:4213–6. doi:10.1021/jz4023865.

[68] Perdew JP, Ernzerhof M, Burke K. Rationale for mixing exact exchange with density functional approximations. J Chem Phys 1996;105:9982–5. doi:doi:http://dx.doi.org/10.1063/1.472933.

[69] Heyd J, Scuseria GE, Ernzerhof M. Hybrid functionals based on a screened Coulomb potential. J Chem Phys 2003;118:8207–15. doi:10.1063/1.1564060.

[70] Meggiolaro D, De Angelis F. First-Principles Modeling of Defects in Lead Halide Perovskites: Best Practices and Open Issues. ACS Energy Lett 2018;3:2206–22. doi:10.1021/acsenergylett.8b01212.

[71] Welch E, Scolfaro L, Zakhidov A. Density functional theory + U modeling of polarons in organohalide lead perovskites. AIP Adv 2016;6:125037. doi:10.1063/1.4972341.

[72] Mosconi E, Merabet B, Meggiolaro D, Zaoui A, De Angelis F. First-Principles Modeling of Bismuth Doping in the MAPbI3 Perovskite. J Phys Chem C 2018;122:14107–12. doi:10.1021/acs.jpcc.8b01307.

[73] Yin W-J, Shi T, Yan Y. Unusual defect physics in CH3NH3PbI3 perovskite solar cell absorber. Appl Phys Lett 2014;104:63903. doi:doi:http://dx.doi.org/10.1063/1.4864778.

[74] Liu N, Yam C. First-principles study of intrinsic defects in formamidinium lead triiodide perovskite solar cell absorbers. Phys Chem Chem Phys 2018;20:6800–4. doi:10.1039/C8CP00280K.

[75] Kang J, Wang L-W. High Defect Tolerance in Lead Halide Perovskite CsPbBr3. J Phys Chem Lett 2017;8:489–93. doi:10.1021/acs.jpclett.6b02800.

[76] Li Y, Zhang C, Zhang X, Huang D, Shen Q, Cheng Y, et al. Intrinsic point defects in inorganic perovskite CsPbI3 from first-principles prediction. Appl Phys Lett 2017;111:162106. doi:10.1063/1.5001535.

[77] Walsh A, Scanlon DO, Chen S, Gong XG, Wei S-H. Self-Regulation Mechanism for Charged Point Defects in Hybrid Halide Perovskites. Angew Chem Int Ed 2014;53:1–5. doi:10.1002/anie.201409740.

[78] Meggiolaro D, Motti SG, Mosconi E, Barker AJ, Ball J, Andrea Riccardo Perini C, et al. Iodine chemistry determines the defect tolerance of lead-halide perovskites. Energy Environ Sci 2018;11:702–13. doi:10.1039/c8ee00124c.

[79] Du M-H. Density Functional Calculations of Native Defects in CH3NH3PbI3: Effects of Spin–Orbit Coupling and Self-Interaction Error. J Phys Chem Lett 2015;6:1461–6. doi:10.1021/acs.jpclett.5b00199.

[80] Azpiroz JM, Mosconi E, Bisquert J, De Angelis F. Defect migration in methylammonium lead iodide and its role in perovskite solar cell operation. Energy Environ Sci 2015;8:2118–27. doi:10.1039/C5EE01265A.

[81] Ming W, Chen S, Du M-H. Chemical instability leads to unusual chemical-potential-independent defect formation and diffusion in perovskite solar cell material CH3NH3PbI3. J Mater Chem A 2016;4:16975–81. doi:10.1039/C6TA07492H.

[82] Shi T, Yin W-JW-J, Yan Y. Predictions for p-Type CH3NH3PbI3 Perovskites. J Phys Chem C 2014;118:25350–4. doi:10.1021/jp508328u.

[83] Liu J, Prezhdo O V. Chlorine Doping Reduces Electron-Hole Recombination in Lead Iodide Perovskites: Time-Domain Ab Initio Analysis. J Phys Chem Lett 2015;6:4463–9. doi:10.1021/acs.jpclett.5b02355.

[84] Meggiolaro D, Mosconi E, De Angelis F. Mechanism of Reversible Trap Passivation by Molecular Oxygen in Lead-Halide Perovskites. ACS Energy Lett 2017:2794–8. doi:10.1021/acsenergylett.7b00955.

[85] Meggiolaro D, Mosconi E, De Angelis F. Modeling the Interaction of Molecular Iodine with MAPbI3: A Probe of Lead-Halide Perovskites Defect Chemistry. ACS Energy Lett 2018;3:447–51. doi:10.1021/acsenergylett.7b01244.

[86] Aristidou N, Eames C, Sanchez-Molina I, Bu X, Kosco J, Islam MS, et al. Fast oxygen diffusion and iodide defects mediate oxygen-induced degradation of perovskite solar cells. Nat Commun 2017;8:15218. doi:10.1038/ncomms15218 https://www.nature.com/articles/ncomms15218#supplementary-information.

[87] Vincent BR, Robertson KN, Cameron TS, Knop O. Alkylammonium lead halides. Part 1. Isolated PbI64− ions in (CH3NH3)4PbI6•2H2O. Can J Chem 1987;65:1042–6. doi:10.1139/v87-176.

[88] Brivio F, Butler KT, Walsh A, van Schilfgaarde M. Relativistic quasiparticle self-consistent electronic structure of hybrid halide perovskite photovoltaic absorbers. Phys Rev B 2014;89:155204. doi:10.1103/PhysRevB.89.155204.

[89] Sadhanala A, Deschler F, Thomas TH, Dutton SE, Goedel KC, Hanusch FC, et al. Preparation of Single-Phase Films of CH3NH3Pb(I1–xBrx)3 with Sharp Optical Band Edges. J Phys Chem Lett 2014;5:2501–5. doi:10.1021/jz501332v.

[90] D'Innocenzo V, Srimath Kandada AR, De Bastiani M, Gandini M, Petrozza A. Tuning the Light Emission Properties by Band Gap Engineering in Hybrid Lead Halide Perovskite. J Am Chem Soc 2014;136:17730–3. doi:10.1021/ja511198f.

[91] Leijtens T, Eperon GE, Noel NK, Habisreutinger SN, Petrozza A, Snaith HJ. Stability of Metal Halide Perovskite Solar Cells. Adv Energy Mater 2015;5:1500963. doi:10.1002/aenm.201500963.

[92] McMeekin DP, Sadoughi G, Rehman W, Eperon GE, Saliba M, Hörantner MT, et al. A mixed-cation lead mixed-halide perovskite absorber for tandem solar cells. Science (80-) 2016;351:151 LP – 155. doi:10.1126/science.aad5845.

[93] Charles B, Dillon J, Weber OJ, Islam MS, Weller MT. Understanding the stability of mixed A-cation lead iodide perovskites. J Mater Chem A 2017;5:22495–9. doi:10.1039/C7TA08617B.

[94] Jeon NJ, Noh JH, Yang WS, Kim YC, Ryu S, Seo J, et al. Compositional engineering of

perovskite materials for high-performance solar cells. Nature 2015;517:476.

[95] Chen J, Messing ME, Zheng K, Pullerits T. Cation-Dependent Hot Carrier Cooling in Halide Perovskite Nanocrystals. J Am Chem Soc 2019;141:3532–40. doi:10.1021/jacs.8b11867.

[96] Hopper TR, Gorodetsky A, Frost JM, Müller C, Lovrincic R, Bakulin AA. Ultrafast Intraband Spectroscopy of Hot-Carrier Cooling in Lead-Halide Perovskites. ACS Energy Lett 2018;3:2199–205. doi:10.1021/acsenergylett.8b01227.

[97] Tan H, Che F, Wei M, Zhao Y, Saidaminov MI, Todorović P, et al. Dipolar cations confer defect tolerance in wide-bandgap metal halide perovskites. Nat Commun 2018;9:3100. doi:10.1038/s41467-018-05531-8.

[98] Bonn M, Miyata K, Hendry E, Zhu X-Y. Role of Dielectric Drag in Polaron Mobility in Lead Halide Perovskites. ACS Energy Lett 2017;2:2555–62. doi:10.1021/acsenergylett.7b00717.

[99] Abate A. Perovskite Solar Cells Go Lead Free. Joule 2017;1:659–64. doi:https://doi.org/10.1016/j.joule.2017.09.007.

[100] Giustino F, Snaith HJ. Toward Lead-Free Perovskite Solar Cells. ACS Energy Lett 2016;1:1233–40. doi:10.1021/acsenergylett.6b00499.

[101] Xiao Z, Meng W, Wang J, Mitzi DB, Yan Y. Searching for promising new perovskite-based photovoltaic absorbers: the importance of electronic dimensionality. Mater Horizons 2017;4:206–16. doi:10.1039/C6MH00519E.

[102] Zhao X-G, Yang D, Ren J-C, Sun Y, Xiao Z, Zhang L. Rational Design of Halide Double Perovskites for Optoelectronic Applications. Joule 2018;2:1662–73. doi:10.1016/j.joule.2018.06.017.

[103] Zhang X, Li L, Sun Z, Luo J. Rational chemical doping of metal halide perovskites. Chem Soc Rev 2019;48:517–39. doi:10.1039/c8cs00563j.

[104] Zhou Y, Chen J, Bakr OM, Sun H-T. Metal-Doped Lead Halide Perovskites: Synthesis, Properties, and Optoelectronic Applications. Chem Mater 2018;30:6589–613. doi:10.1021/acs.chemmater.8b02989.

[105] Noh JH, Im SH, Heo JH, Mandal TN, Seok S Il. Chemical Management for Colorful, Efficient, and Stable Inorganic–Organic Hybrid Nanostructured Solar Cells. Nano Lett 2013;13:1764–9. doi:10.1021/nl400349b.

[106] Xing G, Mathews N, Lim SS, Yantara N, Liu X, Sabba D, et al. Low-temperature solution-processed wavelength-tunable perovskites for lasing. Nat Mater 2014;13:476.

[107] Zhu H, Fu Y, Meng F, Wu X, Gong Z, Ding Q, et al. Lead halide perovskite nanowire lasers with low lasing thresholds and high quality factors. Nat Mater 2015;14:636.

[108] Wu B, Yuan H, Xu Q, Steele JA, Giovanni D, Puech P, et al. Indirect tail states formation by thermal-induced polar fluctuations in halide perovskites. Nat Commun 2019;10:484. doi:10.1038/s41467-019-08326-7.

[109] Fu J, Jamaludin NF, Wu B, Li M, Solanki A, Ng YF, et al. Localized Traps Limited Recombination in Lead Bromide Perovskites. Adv Energy Mater 2019;0:1803119. doi:10.1002/aenm.201803119.

[110] Hieulle J, Wang X, Stecker C, Son D-Y, Qiu L, Ohmann R, et al. Unraveling the Impact of Halide Mixing on Perovskite Stability. J Am Chem Soc 2019;141:3515–23. doi:10.1021/jacs.8b11210.

[111] Yin W-J, Yan Y, Wei S-H. Anomalous Alloy Properties in Mixed Halide Perovskites. J Phys Chem Lett 2014;5:3625–31. doi:10.1021/jz501896w.

[112] Wei H, DeSantis D, Wei W, Deng Y, Guo D, Savenije TJ, et al. Dopant compensation in alloyed CH3NH3PbBr3−xClx perovskite single crystals for gamma-ray spectroscopy. Nat Mater 2017;16:826.

[113] Lee MM, Teuscher J, Miyasaka T, Murakami TN, Snaith HJ. Efficient Hybrid Solar Cells Based on Meso-Superstructured Organometal Halide Perovskites. Science (80-) 2012;338:643 LP – 647. doi:10.1126/science.1228604.

[114] Stranks SD, Eperon GE, Grancini G, Menelaou C, Alcocer MJP, Leijtens T, et al. Electron-Hole Diffusion Lengths Exceeding 1 Micrometer in an Organometal Trihalide Perovskite

Absorber. Science (80-) 2013;342:341 LP – 344. doi:10.1126/science.1243982.

[115] Xing G, Mathews N, Sun S, Lim SS, Lam YM, Grätzel M, et al. Long-Range Balanced Electron- and Hole-Transport Lengths in Organic-Inorganic CH3NH3PbI3. Science (80-) 2013;342:344 LP – 347. doi:10.1126/science.1243167.

[116] Chen Q, Zhou H, Fang Y, Stieg AZ, Song T-B, Wang H-H, et al. The optoelectronic role of chlorine in CH3NH3PbI3(Cl)-based perovskite solar cells. Nat Commun 2015;6:7269.

[117] Fan L, Ding Y, Luo J, Shi B, Yao X, Wei C, et al. Elucidating the role of chlorine in perovskite solar cells. J Mater Chem A 2017;5:7423–32. doi:10.1039/C7TA00973A.

[118] Dohner ER, Jaffe A, Bradshaw LR, Karunadasa HI. Intrinsic White-Light Emission from Layered Hybrid Perovskites. J Am Chem Soc 2014;136:13154–7. doi:10.1021/ja507086b.

[119] Smith MD, Connor BA, Karunadasa HI. Tuning the Luminescence of Layered Halide Perovskites. Chem Rev 2019. doi:10.1021/acs.chemrev.8b00477.

[120] Jang DM, Park K, Kim DH, Park J, Shojaei F, Kang HS, et al. Reversible Halide Exchange Reaction of Organometal Trihalide Perovskite Colloidal Nanocrystals for Full-Range Band Gap Tuning. Nano Lett 2015;15:5191–9. doi:10.1021/acs.nanolett.5b01430.

[121] Zhang F, Zhong H, Chen C, Wu X, Hu X, Huang H, et al. Brightly Luminescent and Color-Tunable Colloidal CH3NH3PbX3 (X = Br, I, Cl) Quantum Dots: Potential Alternatives for Display Technology. ACS Nano 2015;9:4533–42. doi:10.1021/acsnano.5b01154.

[122] Protesescu L, Yakunin S, Bodnarchuk MI, Krieg F, Caputo R, Hendon CH, et al. Nanocrystals of Cesium Lead Halide Perovskites (CsPbX3, X = Cl, Br, and I): Novel Optoelectronic Materials Showing Bright Emission with Wide Color Gamut. Nano Lett 2015;15:3692–6. doi:10.1021/nl5048779.

[123] Nedelcu G, Protesescu L, Yakunin S, Bodnarchuk MI, Grotevent MJ, Kovalenko M V. Fast Anion-Exchange in Highly Luminescent Nanocrystals of Cesium Lead Halide Perovskites (CsPbX3, X = Cl, Br, I). Nano Lett 2015;15:5635–40. doi:10.1021/acs.nanolett.5b02404.

[124] Akkerman QA, D'Innocenzo V, Accornero S, Scarpellini A, Petrozza A, Prato M, et al.

Tuning the Optical Properties of Cesium Lead Halide Perovskite Nanocrystals by Anion Exchange Reactions. J Am Chem Soc 2015;137:10276–81. doi:10.1021/jacs.5b05602.

[125] Shamsi J, Urban AS, Imran M, De Trizio L, Manna L. Metal Halide Perovskite Nanocrystals: Synthesis, Post-Synthesis Modifications, and Their Optical Properties. Chem Rev 2019. doi:10.1021/acs.chemrev.8b00644.

[126] Parobek D, Dong Y, Qiao T, Rossi D, Son DH. Photoinduced Anion Exchange in Cesium Lead Halide Perovskite Nanocrystals. J Am Chem Soc 2017;139:4358–61. doi:10.1021/jacs.7b01480.

[127] Guhrenz C, Benad A, Ziegler C, Haubold D, Gaponik N, Eychmüller A. Solid-State Anion Exchange Reactions for Color Tuning of CsPbX3 Perovskite Nanocrystals. Chem Mater 2016;28:9033–40. doi:10.1021/acs.chemmater.6b03980.

[128] Hoffman JB, Schleper AL, Kamat P V. Transformation of Sintered CsPbBr3 Nanocrystals to Cubic CsPbI3 and Gradient CsPbBrxI3–x through Halide Exchange. J Am Chem Soc 2016;138:8603–11. doi:10.1021/jacs.6b04661.

[129] Koscher BA, Bronstein ND, Olshansky JH, Bekenstein Y, Alivisatos AP. Surface- vs Diffusion-Limited Mechanisms of Anion Exchange in CsPbBr3 Nanocrystal Cubes Revealed through Kinetic Studies. J Am Chem Soc 2016;138:12065–8. doi:10.1021/jacs.6b08178.

[130] Unger EL, Hoke ET, Bailie CD, Nguyen WH, Bowring AR, Heumüller T, et al. Hysteresis and transient behavior in current–voltage measurements of hybrid-perovskite absorber solar cells. Energy Environ Sci 2014;7:3690–8. doi:10.1039/C4EE02465F.

[131] Hoke ET, Slotcavage DJ, Dohner ER, Bowring AR, Karunadasa HI, McGehee MD. Reversible photo-induced trap formation in mixed-halide hybrid perovskites for photovoltaics. Chem Sci 2015;6:613–7. doi:10.1039/C4SC03141E.

[132] De Bastiani M, Dell'Erba G, Gandini M, D'Innocenzo V, Neutzner S, Kandada ARS, et al. Ion Migration and the Role of Preconditioning Cycles in the Stabilization of the J–V Characteristics of Inverted Hybrid Perovskite Solar Cells. Adv Energy Mater

2016;6:1501453. doi:10.1002/aenm.201501453.

[133] Rizzo A, Lamberti F, Buonomo M, Wrachien N, Torto L, Lago N, et al. Understanding lead iodide perovskite hysteresis and degradation causes by extensive electrical characterization. Sol Energy Mater Sol Cells 2019;189:43–52. doi:https://doi.org/10.1016/j.solmat.2018.09.021.

[134] Knight AJ, Wright AD, Patel JB, McMeekin DP, Snaith HJ, Johnston MB, et al. Electronic Traps and Phase Segregation in Lead Mixed-Halide Perovskite. ACS Energy Lett 2019;4:75–84. doi:10.1021/acsenergylett.8b02002.

[135] Brennan MC, Draguta S, Kamat P V, Kuno M. Light-Induced Anion Phase Segregation in Mixed Halide Perovskites. ACS Energy Lett 2018;3:204–13. doi:10.1021/acsenergylett.7b01151.

[136] Davies CL, Filip MR, Patel JB, Crothers TW, Verdi C, Wright AD, et al. Bimolecular recombination in methylammonium lead triiodide perovskite is an inverse absorption process. Nat Commun 2018;9:293. doi:10.1038/s41467-017-02670-2.

[137] Yang Y, Ostrowski DP, France RM, Zhu K, van de Lagemaat J, Luther JM, et al. Observation of a hot-phonon bottleneck in lead-iodide perovskites. Nat Photonics 2015;10:53.

[138] Manser JS, Christians JA, Kamat P V. Intriguing Optoelectronic Properties of Metal Halide Perovskites. Chem Rev 2016;116:12956–3008. doi:10.1021/acs.chemrev.6b00136.

[139] D'Innocenzo V, Grancini G, Alcocer MJP, Kandada ARS, Stranks SD, Lee MM, et al. Excitons versus free charges in organo-lead tri-halide perovskites. Nat Commun 2014;5:3586.

[140] Norris DJ, Efros AL, Erwin SC. Doped Nanocrystals. Science (80-) 2008;319:1776 LP – 1779. doi:10.1126/science.1143802.

[141] Zhou Y, Chen J, Bakr OM, Sun H-T. Metal-Doped Lead Halide Perovskites: Synthesis, Properties, and Optoelectronic Applications. Chem Mater 2018;30:6589–613.

doi:10.1021/acs.chemmater.8b02989.

[142] Yin J, Ahmed GH, Bakr OM, Brédas J-L, Mohammed OF. Unlocking the Effect of Trivalent Metal Doping in All-Inorganic CsPbBr3 Perovskite. ACS Energy Lett 2019:789–95. doi:10.1021/acsenergylett.9b00209.

[143] Pretty MC. Molecular Electronics: from Principles to Practice. Wiley; 2007. doi:10.1002/9780470723890.fmatter.

[144] Lüssem B, Riede M, Leo K. Doping of organic semiconductors. Phys Status Solidi 2013;210:9–43. doi:10.1002/pssa.201228310.

[145] Beaulac R, Archer PI, Ochsenbein ST, Gamelin DR. Mn2+-Doped CdSe Quantum Dots: New Inorganic Materials for Spin-Electronics and Spin-Photonics. Adv Funct Mater 2008;18:3873–91. doi:10.1002/adfm.200801016.

[146] Pradhan N, Peng X. Efficient and Color-Tunable Mn-Doped ZnSe Nanocrystal Emitters: Control of Optical Performance via Greener Synthetic Chemistry. J Am Chem Soc 2007;129:3339–47. doi:10.1021/ja068360v.

[147] Beaulac R, Archer PI, van Rijssel J, Meijerink A, Gamelin DR. Exciton Storage by Mn2+ in Colloidal Mn2+-Doped CdSe Quantum Dots. Nano Lett 2008;8:2949–53. doi:10.1021/nl801847e.

[148] Liu H, Wu Z, Shao J, Yao D, Gao H, Liu Y, et al. CsPbxMn1–xCl3 Perovskite Quantum Dots with High Mn Substitution Ratio. ACS Nano 2017;11:2239–47. doi:10.1021/acsnano.6b08747.

[149] Liu W, Lin Q, Li H, Wu K, Robel I, Pietryga JM, et al. Mn2+-Doped Lead Halide Perovskite Nanocrystals with Dual-Color Emission Controlled by Halide Content. J Am Chem Soc 2016;138:14954–61. doi:10.1021/jacs.6b08085.

[150] Parobek D, Roman BJ, Dong Y, Jin H, Lee E, Sheldon M, et al. Exciton-to-Dopant Energy Transfer in Mn-Doped Cesium Lead Halide Perovskite Nanocrystals. Nano Lett 2016;16:7376–80. doi:10.1021/acs.nanolett.6b02772.

[151] Pinchetti V, Anand A, Akkerman QA, Sciacca D, Lorenzon M, Meinardi F, et al. Trap-Mediated Two-Step Sensitization of Manganese Dopants in Perovskite Nanocrystals. ACS Energy Lett 2019;4:85–93. doi:10.1021/acsenergylett.8b02052.

[152] Yuan X, Ji S, De Siena MC, Fei L, Zhao Z, Wang Y, et al. Photoluminescence Temperature Dependence, Dynamics, and Quantum Efficiencies in Mn2+-Doped CsPbCl3 Perovskite Nanocrystals with Varied Dopant Concentration. Chem Mater 2017;29:8003–11. doi:10.1021/acs.chemmater.7b03311.

[153] Xu K, Meijerink A. Tuning Exciton–Mn2+ Energy Transfer in Mixed Halide Perovskite Nanocrystals. Chem Mater 2018;30:5346–52. doi:10.1021/acs.chemmater.8b02157.

[154] van der Stam W, Geuchies JJ, Altantzis T, van den Bos KHW, Meeldijk JD, Van Aert S, et al. Highly Emissive Divalent-Ion-Doped Colloidal CsPb1–xMxBr3 Perovskite Nanocrystals through Cation Exchange. J Am Chem Soc 2017;139:4087–97. doi:10.1021/jacs.6b13079.

[155] Mir WJ, Jagadeeswararao M, Das S, Nag A. Colloidal Mn-Doped Cesium Lead Halide Perovskite Nanoplatelets. ACS Energy Lett 2017;2:537–43. doi:10.1021/acsenergylett.6b00741.

[156] Das Adhikari S, Dutta A, Dutta SK, Pradhan N. Layered Perovskites L2(Pb1–xMnx)Cl4 to Mn-Doped CsPbCl3 Perovskite Platelets. ACS Energy Lett 2018;3:1247–53. doi:10.1021/acsenergylett.8b00653.

[157] Luo B, Li F, Xu K, Guo Y, Liu Y, Xia Z, et al. B-Site doped lead halide perovskites: synthesis, band engineering, photophysics, and light emission applications. J Mater Chem C 2019. doi:10.1039/C8TC05741A.

[158] Rossi D, Parobek D, Dong Y, Son DH. Dynamics of Exciton–Mn Energy Transfer in Mn-Doped CsPbCl3 Perovskite Nanocrystals. J Phys Chem C 2017;121:17143–9. doi:10.1021/acs.jpcc.7b06182.

[159] Righetto M, Minotto A, Bozio R. Bridging Energetics and Dynamics of Exciton Trapping in Core–Shell Quantum Dots. J Phys Chem C 2017;121:896–902.

doi:10.1021/acs.jpcc.6b10146.

[160] Mooney J, Krause MM, Saari JI, Kambhampati P. Challenge to the deep-trap model of the surface in semiconductor nanocrystals. Phys Rev B 2013;87:81201. doi:10.1103/PhysRevB.87.081201.

[161] Hou S, Gangishetty MK, Quan Q, Congreve DN. Efficient Blue and White Perovskite Light-Emitting Diodes via Manganese Doping. Joule 2018;2:2421–33. doi:https://doi.org/10.1016/j.joule.2018.08.005.

[162] Zhou C, Tian Y, Khabou O, Worku M, Zhou Y, Hurley J, et al. Manganese-Doped One-Dimensional Organic Lead Bromide Perovskites with Bright White Emissions. ACS Appl Mater Interfaces 2017;9:40446–51. doi:10.1021/acsami.7b12456.

[163] Parobek D, Dong Y, Qiao T, Son DH. Direct Hot-Injection Synthesis of Mn-Doped CsPbBr3 Nanocrystals. Chem Mater 2018;30:2939–44. doi:10.1021/acs.chemmater.8b00310.

[164] Jellicoe TC, Richter JM, Glass HFJ, Tabachnyk M, Brady R, Dutton SE, et al. Synthesis and Optical Properties of Lead-Free Cesium Tin Halide Perovskite Nanocrystals. J Am Chem Soc 2016;138:2941–4. doi:10.1021/jacs.5b13470.

[165] Bi C, Wang S, Li Q, Kershaw S V, Tian J, Rogach AL. Thermally Stable Copper(II)-Doped Cesium Lead Halide Perovskite Quantum Dots with Strong Blue Emission. J Phys Chem Lett 2019:943–52. doi:10.1021/acs.jpclett.9b00290.

[166] Yong Z-J, Guo S-Q, Ma J-P, Zhang J-Y, Li Z-Y, Chen Y-M, et al. Doping-Enhanced Short-Range Order of Perovskite Nanocrystals for Near-Unity Violet Luminescence Quantum Yield. J Am Chem Soc 2018;140:9942–51. doi:10.1021/jacs.8b04763.

[167] Yamada Y, Hoyano M, Akashi R, Oto K, Kanemitsu Y. Impact of Chemical Doping on Optical Responses in Bismuth-Doped CH3NH3PbBr3 Single Crystals: Carrier Lifetime and Photon Recycling. J Phys Chem Lett 2017;8:5798–803. doi:10.1021/acs.jpclett.7b02508.

[168] Lozhkina OA, Murashkina AA, Shilovskikh V V, Kapitonov Y V, Ryabchuk VK, Emeline A V, et al. Invalidity of Band-Gap Engineering Concept for Bi3+ Heterovalent Doping in

CsPbBr3 Halide Perovskite. J Phys Chem Lett 2018;9:5408–11. doi:10.1021/acs.jpclett.8b02178.

[169] Begum R, Parida MR, Abdelhady AL, Murali B, Alyami NM, Ahmed GH, et al. Engineering Interfacial Charge Transfer in CsPbBr3 Perovskite Nanocrystals by Heterovalent Doping. J Am Chem Soc 2017;139:731–7. doi:10.1021/jacs.6b09575.

[170] Zou S, Yang G, Yang T, Zhao D, Gan Z, Chen W, et al. Template-Free Synthesis of High-Yield Fe-Doped Cesium Lead Halide Perovskite Ultralong Microwires with Enhanced Two-Photon Absorption. J Phys Chem Lett 2018;9:4878–85. doi:10.1021/acs.jpclett.8b02127.

[171] Liu M, Zhong G, Yin Y, Miao J, Li K, Wang C, et al. Aluminum-Doped Cesium Lead Bromide Perovskite Nanocrystals with Stable Blue Photoluminescence Used for Display Backlight. Adv Sci 2017;4:1700335. doi:10.1002/advs.201700335.

[172] Abdelhady AL, Saidaminov MI, Murali B, Adinolfi V, Voznyy O, Katsiev K, et al. Heterovalent Dopant Incorporation for Bandgap and Type Engineering of Perovskite Crystals. J Phys Chem Lett 2016;7:295–301. doi:10.1021/acs.jpclett.5b02681.

[173] Nayak PK, Sendner M, Wenger B, Wang Z, Sharma K, Ramadan AJ, et al. Impact of Bi3+ Heterovalent Doping in Organic–Inorganic Metal Halide Perovskite Crystals. J Am Chem Soc 2018;140:574–7. doi:10.1021/jacs.7b11125.

[174] Meng R, Wu G, Zhou J, Zhou H, Fang H, Loi MA, et al. Understanding the Impacts of Bismuth Heterovalent Doping on the Structural and Photophysical Properties in CH3NH3PbBr3 Halide Perovskite Crystals with Near-IR Photoluminescence. Chem – A Eur J 2019;0. doi:10.1002/chem.201805370.

[175] Harikesh PC, Wu B, Ghosh B, John RA, Lie S, Thirumal K, et al. Doping and Switchable Photovoltaic Effect in Lead-Free Perovskites Enabled by Metal Cation Transmutation. Adv Mater 2018. doi:10.1002/adma.201802080.

[176] Nayak PK, Sendner M, Wenger B, Wang Z, Sharma K, Ramadan AJ, et al. Impact of Bi3+ Heterovalent Doping in Organic-Inorganic Metal Halide Perovskite Crystals. J Am Chem

Soc 2018;140:574–7. doi:10.1021/jacs.7b11125.

[177] Yao J-S, Ge J, Han B-N, Wang K-H, Yao H-B, Yu H-L, et al. Ce3+-Doping to Modulate Photoluminescence Kinetics for Efficient CsPbBr3 Nanocrystals Based Light-Emitting Diodes. J Am Chem Soc 2018;140:3626–34. doi:10.1021/jacs.7b11955.

[178] Zhou D, Liu D, Pan G, Chen X, Li D, Xu W, et al. Cerium and Ytterbium Codoped Halide Perovskite Quantum Dots: A Novel and Efficient Downconverter for Improving the Performance of Silicon Solar Cells. Adv Mater 2017;29:1704149. doi:10.1002/adma.201704149.

[179] Kroupa DM, Roh JY, Milstein TJ, Creutz SE, Gamelin DR. Quantum-Cutting Ytterbium-Doped CsPb(Cl1–xBrx)3 Perovskite Thin Films with Photoluminescence Quantum Yields over 190%. ACS Energy Lett 2018;3:2390–5. doi:10.1021/acsenergylett.8b01528.

[180] Milstein TJ, Kroupa DM, Gamelin DR. Picosecond Quantum Cutting Generates Photoluminescence Quantum Yields Over 100% in Ytterbium-Doped CsPbCl3 Nanocrystals. Nano Lett 2018;18:3792–9. doi:10.1021/acs.nanolett.8b01066.

[181] Milstein TJ, Kluherz KT, Kroupa DM, Erickson CS, De Yoreo JJ, Gamelin DR. Anion Exchange and the Quantum-Cutting Energy Threshold in Ytterbium-Doped CsPb(Cl1–xBrx)3 Perovskite Nanocrystals. Nano Lett 2019. doi:10.1021/acs.nanolett.8b05104.

[182] Luo X, Ding T, Liu X, Liu Y, Wu K. Quantum-Cutting Luminescent Solar Concentrators Using Ytterbium-Doped Perovskite Nanocrystals. Nano Lett 2019;19:338–41. doi:10.1021/acs.nanolett.8b03966.

[183] Pan G, Bai X, Yang D, Chen X, Jing P, Qu S, et al. Doping Lanthanide into Perovskite Nanocrystals: Highly Improved and Expanded Optical Properties. Nano Lett 2017;17:8005–11. doi:10.1021/acs.nanolett.7b04575.

[184] Ahmed GH, El-Demellawi JK, Yin J, Pan J, Velusamy DB, Hedhili MN, et al. Giant Photoluminescence Enhancement in CsPbCl3 Perovskite Nanocrystals by Simultaneous Dual-Surface Passivation. ACS Energy Lett 2018;3:2301–7.

doi:10.1021/acsenergylett.8b01441.

[185] Mamishev A V, Sundara-Rajan K, Yang F, Du Y, Zahn M. Interdigital sensors and transducers. Proc IEEE 2004;92:808–45. doi:10.1109/JPROC.2004.826603.

[186] Søndergaard RR, Hösel M, Krebs FC. Roll-to-Roll fabrication of large area functional organic materials. J Polym Sci Part B Polym Phys 2013;51:16–34. doi:10.1002/polb.23192.

[187] Wang S, Kaienburg P, Klingebiel B, Schillings D, Kirchartz T. Understanding Thermal Admittance Spectroscopy in Low-Mobility Semiconductors. J Phys Chem C 2018;122:9795–803. doi:10.1021/acs.jpcc.8b01921.

[188] Rizzo A, Cester A, Wrachien N, Lago N, Torto L, Barbato M, et al. Characterization and modeling of organic (P3HT:PCBM) solar cells as a function of bias and illumination. Sol Energy Mater Sol Cells 2016;157:337–45. doi:https://doi.org/10.1016/j.solmat.2016.06.001.

[189] Garcia-Belmonte G, Boix PP, Bisquert J, Sessolo M, Bolink HJ. Simultaneous determination of carrier lifetime and electron density-of-states in P3HT:PCBM organic solar cells under illumination by impedance spectroscopy. Sol Energy Mater Sol Cells 2010;94:366–75. doi:https://doi.org/10.1016/j.solmat.2009.10.015.

[190] Almora O, Aranda C, Mas-Marzá E, Garcia-Belmonte G. On Mott-Schottky analysis interpretation of capacitance measurements in organometal perovskite solar cells. Appl Phys Lett 2016;109:173903. doi:10.1063/1.4966127.

[191] Jung EH, Jeon NJ, Park EY, Moon CS, Shin TJ, Yang T-Y, et al. Efficient, stable and scalable perovskite solar cells using poly(3-hexylthiophene). Nature 2019;567:511–5. doi:10.1038/s41586-019-1036-3.

[192] Lago N, Cester A, Wrachien N, Benvenuti E, Quiroga SD, Natali M, et al. Investigation of Mobility Transient on Organic Transistor by Means of DLTS Technique. IEEE Trans Electron Devices 2016;63:4432–9. doi:10.1109/TED.2016.2611142.

[193] Heo S, Seo G, Lee Y, Lee D, Seol M, Lee J, et al. Deep level trapped defect analysis in $CH_3NH_3PbI_3$ perovskite solar cells by deep level transient spectroscopy. Energy Environ Sci

2017;10:1128–33. doi:10.1039/C7EE00303J.

[194] Walter D, Fell A, Wu Y, Duong T, Barugkin C, Wu N, et al. Transient Photovoltage in Perovskite Solar Cells: Interaction of Trap-Mediated Recombination and Migration of Multiple Ionic Species. J Phys Chem C 2018;122:11270–81. doi:10.1021/acs.jpcc.8b02529.

[195] Bi D, Moon S-J, Häggman L, Boschloo G, Yang L, Johansson EMJ, et al. Using a two-step deposition technique to prepare perovskite (CH3NH3PbI3) for thin film solar cells based on ZrO2 and TiO2 mesostructures. RSC Adv 2013;3:18762. doi:10.1039/c3ra43228a.

[196] Muller RS, Kamins TI, Chan M. Device electronics for integrated circuits. John Wiley & Sons; 2003.

[197] Kirchartz T, Gong W, Hawks SA, Agostinelli T, MacKenzie RCI, Yang Y, et al. Sensitivity of the Mott–Schottky Analysis in Organic Solar Cells. J Phys Chem C 2012;116:7672–80. doi:10.1021/jp300397f.

[198] Barsoukov E, Macdonald JR. Impedance Spectroscopy: Theory, Experiment, and Applications. 2005. doi:10.1002/0471716243.

[199] Torto L, Cester A, Wrachien N, Rizzo A, Gedefaw D, Andersson MR, et al. Application of an Open-Circuit Voltage Decay Model to Compare the Performances of Donor Polymers in Bulk Heterojunction Solar Cells. IEEE J Photovoltaics 2018;8:517–24. doi:10.1109/JPHOTOV.2018.2792461.

[200] Rose A. Space-Charge-Limited Currents in Solids. Phys Rev 1955;97:1538–44. doi:10.1103/PhysRev.97.1538.

[201] Wang Z, McMeekin DP, Sakai N, van Reenen S, Wojciechowski K, Patel JB, et al. Efficient and Air-Stable Mixed-Cation Lead Mixed-Halide Perovskite Solar Cells with n-Doped Organic Electron Extraction Layers. Adv Mater 2017;29. doi:10.1002/adma.201604186.

[202] Xiao Z, Yuan Y, Shao Y, Wang Q, Dong Q, Bi C, et al. Giant switchable photovoltaic effect in organometal trihalide perovskite devices. Nat Mater 2014;14:193.

[203] Son D-Y, Kim S-G, Seo J-Y, Lee S-H, Shin H, Lee D, et al. Universal Approach toward

Hysteresis-Free Perovskite Solar Cell via Defect Engineering. J Am Chem Soc 2018;140:1358–64. doi:10.1021/jacs.7b10430.

[204] Lamberti F, Gatti T, Cescon E, Sorrentino R, Rizzo A, Menna E, et al. Evidence of Spiro-OMeTAD De-doping by tert-Butylpyridine Additive in Hole-Transporting Layers for Perovskite Solar Cells. Chem 2019. doi:10.1016/j.chempr.2019.04.003.

[205] Zhang H, Ren X, Chen X, Mao J, Cheng J, Zhao Y, et al. Improving the stability and performance of perovskite solar cells via off-the-shelf post-device ligand treatment. Energy Environ Sci 2018;11:2253–62. doi:10.1039/C8EE00580J.

[206] Gatti T, Vicentini N, Mba M, Menna E. Organic Functionalized Carbon Nanostructures for Functional Polymer-Based Nanocomposites. Eur J Org Chem 2016;2016:1071–90. doi:doi:10.1002/ejoc.201501411.

[207] Cheng Z, Lin J. Layered organic–inorganic hybrid perovskites: structure, optical properties, film preparation, patterning and templating engineering. CrystEngComm 2010;12:2646–62. doi:10.1039/C001929A.

[208] Xue Q, Hu Z, Sun C, Chen Z, Huang F, Yip H-L, et al. Metallohalide perovskite–polymer composite film for hybrid planar heterojunction solar cells. RSC Adv 2015;5:775–83. doi:10.1039/C4RA11739E.

[209] Chang C-Y, Chu C-Y, Huang Y-C, Huang C-W, Chang S-Y, Chen C-A, et al. Tuning Perovskite Morphology by Polymer Additive for High Efficiency Solar Cell. ACS Appl Mater Interfaces 2015;7:4955–61. doi:10.1021/acsami.5b00052.

[210] Ding Y, Yao X, Zhang X, Wei C, Zhao Y. Surfactant enhanced surface coverage of CH3NH3PbI3−xClx perovskite for highly efficient mesoscopic solar cells. J Power Sources 2014;272:351–5. doi:https://doi.org/10.1016/j.jpowsour.2014.08.095.

[211] Masi S, Colella S, Listorti A, Roiati V, Liscio A, Palermo V, et al. Growing perovskite into polymers for easy-processable optoelectronic devices. Sci Rep 2015;5:7725.

[212] Masi S, Rizzo A, Aiello F, Balzano F, Uccello-Barretta G, Listorti A, et al. Multiscale

morphology design of hybrid halide perovskites through a polymeric template. Nanoscale 2015;7:18956–63. doi:10.1039/c5nr04715c.

[213] Giuri A, Masi S, Listorti A, Gigli G, Colella S, Esposito Corcione C, et al. Polymeric rheology modifier allows single-step coating of perovskite ink for highly efficient and stable solar cells. Nano Energy 2018;54:400–8. doi:10.1016/j.nanoen.2018.10.039.

[214] Masi S, Aiello F, Listorti A, Balzano F, Altamura D, Giannini C, et al. Connecting the solution chemistry of PbI2 and MAI: A cyclodextrin-based supramolecular approach to the formation of hybrid halide perovskites. Chem Sci 2018;9:3200–8. doi:10.1039/c7sc05095j.

[215] Zhou Q, Bai Z, Lu W-G, Wang Y, Zou B, Zhong H. In Situ Fabrication of Halide Perovskite Nanocrystal-Embedded Polymer Composite Films with Enhanced Photoluminescence for Display Backlights. Adv Mater 2016;28:9163–8. doi:10.1002/adma.201602651.

[216] Raja SN, Bekenstein Y, Koc MA, Fischer S, Zhang D, Lin L, et al. Encapsulation of Perovskite Nanocrystals into Macroscale Polymer Matrices: Enhanced Stability and Polarization. ACS Appl Mater Interfaces 2016;8:35523–33. doi:10.1021/acsami.6b09443.

[217] Wei Y, Deng X, Xie Z, Cai X, Liang S, Ma P, et al. Enhancing the Stability of Perovskite Quantum Dots by Encapsulation in Crosslinked Polystyrene Beads via a Swelling–Shrinking Strategy toward Superior Water Resistance. Adv Funct Mater 2017;27. doi:10.1002/adfm.201703535.

[218] Pan A, Jurow MJ, Qiu F, Yang J, Ren B, Urban JJ, et al. Nanorod Suprastructures from a Ternary Graphene Oxide-Polymer-CsPbX3 Perovskite Nanocrystal Composite That Display High Environmental Stability. Nano Lett 2017;17:6759–65. doi:10.1021/acs.nanolett.7b02959.

[219] Ma K, Du X-Y, Zhang Y-W, Chen S. In situ fabrication of halide perovskite nanocrystals embedded in polymer composites via microfluidic spinning microreactors. J Mater Chem C 2017;5:9398–404. doi:10.1039/c7tc02847d.

[220] Xin Y, Zhao H, Zhang J. Highly Stable and Luminescent Perovskite-Polymer Composites

from a Convenient and Universal Strategy. ACS Appl Mater Interfaces 2018;10:4971–80. doi:10.1021/acsami.7b16442.

[221] Wang Y, Varadi L, Trinchi A, Shen J, Zhu Y, Wei G, et al. Spray-Assisted Coil–Globule Transition for Scalable Preparation of Water-Resistant CsPbBr<inf>3</inf>@PMMA Perovskite Nanospheres with Application in Live Cell Imaging. Small 2018;14. doi:10.1002/smll.201803156.

[222] Li J, Bade SGR, Shan X, Yu Z. Single-Layer Light-Emitting Diodes Using Organometal Halide Perovskite/Poly(ethylene oxide) Composite Thin Films. Adv Mater 2015;27:5196–202. doi:10.1002/adma.201502490.

[223] Bade SGR, Shan X, Hoang PT, Li J, Geske T, Cai L, et al. Stretchable Light-Emitting Diodes with Organometal-Halide-Perovskite–Polymer Composite Emitters. Adv Mater 2017;29. doi:10.1002/adma.201607053.

[224] Xu L, Meng Y, Xu C, Chen P. Room temperature two-photon-pumped random lasers in FAPbBr3/polyethylene oxide (PEO) composite perovskite thin film. RSC Adv 2018;8:36910–4. doi:10.1039/c8ra07452f.

[225] Yao E-P, Yang Z, Meng L, Sun P, Dong S, Yang Y, et al. High-Brightness Blue and White LEDs based on Inorganic Perovskite Nanocrystals and their Composites. Adv Mater 2017;29. doi:10.1002/adma.201606859.

[226] Lin CC, Jiang D-H, Kuo C-C, Cho C-J, Tsai Y-H, Satoh T, et al. Water-Resistant Efficient Stretchable Perovskite-Embedded Fiber Membranes for Light-Emitting Diodes. ACS Appl Mater Interfaces 2018;10:2210–5. doi:10.1021/acsami.7b15989.

[227] Ding R, Zhang X, Chen G, Wang H, Kishor R, Xiao J, et al. High-performance piezoelectric nanogenerators composed of formamidinium lead halide perovskite nanoparticles and poly(vinylidene fluoride). Nano Energy 2017;37:126–35. doi:10.1016/j.nanoen.2017.05.010.

[228] Sultana A, Sadhukhan P, Alam MM, Das S, Middya TR, Mandal D. Organo-Lead Halide Perovskite Induced Electroactive β-Phase in Porous PVDF Films: An Excellent Material for

Photoactive Piezoelectric Energy Harvester and Photodetector. ACS Appl Mater Interfaces 2018;10:4121–30. doi:10.1021/acsami.7b17408.

[229] Shan X, Zhang S, Zhou M, Geske T, Davis M, Hao A, et al. Porous Halide Perovskite–Polymer Nanocomposites for Explosive Detection with a High Sensitivity. Adv Mater Interfaces 2018. doi:10.1002/admi.201801686.

[230] Li H, Shan X, Neu JN, Geske T, Davis M, Mao P, et al. Lead-free halide double perovskite-polymer composites for flexible X-ray imaging. J Mater Chem C 2018;6:11961–7. doi:10.1039/c8tc01564c.

[231] Li J, Shen Y, Liu Y, Shi F, Ren X, Niu T, et al. Stable High-Performance Flexible Photodetector Based on Upconversion Nanoparticles/Perovskite Microarrays Composite. ACS Appl Mater Interfaces 2017;9:19176–83. doi:10.1021/acsami.7b03229.

[232] Yang B, Wang Y, Wei T, Pan Y, Zhou E, Yuan Z, et al. Solution-Processable Near-Infrared–Responsive Composite of Perovskite Nanowires and Photon-Upconversion Nanoparticles. Adv Funct Mater 2018;28. doi:10.1002/adfm.201801782.

[233] Sun H, Tian W, Cao F, Xiong J, Li L. Ultrahigh-Performance Self-Powered Flexible Double-Twisted Fibrous Broadband Perovskite Photodetector. Adv Mater 2018;30:1706986. doi:10.1002/adma.201706986.

[234] Bao C, Zhu W, Yang J, Li F, Gu S, Wang Y, et al. Highly Flexible Self-Powered Organolead Trihalide Perovskite Photodetectors with Gold Nanowire Networks as Transparent Electrodes. ACS Appl Mater Interfaces 2016;8:23868–75. doi:10.1021/acsami.6b08318.

[235] Zhang F, Shi Z-F, Ma Z-Z, Li Y, Li S, Wu D, et al. Silica coating enhances the stability of inorganic perovskite nanocrystals for efficient and stable down-conversion in white light-emitting devices. Nanoscale 2018;10:20131–9. doi:10.1039/c8nr07022a.

[236] Chen D, Yuan S, Chen X, Li J, Mao Q, Li X, et al. CsPbX<inf>3</inf> (X = Br, I) perovskite quantum dot embedded low-melting phosphosilicate glasses: Controllable crystallization, thermal stability and tunable emissions. J Mater Chem C 2018;6:6832–9.

doi:10.1039/c8tc02407c.

[237] Lin H, Tian P, Luo C, Wang H, Zhang J, Yang J, et al. Luminescent Nanofluids of Organometal Halide Perovskite Nanocrystals in Silicone Oils with Ultrastability. ACS Appl Mater Interfaces 2018;10:27244–51. doi:10.1021/acsami.8b05489.

[238] Wang W, Tadé MO, Shao Z. Research progress of perovskite materials in photocatalysis- and photovoltaics-related energy conversion and environmental treatment. Chem Soc Rev 2015;44:5371–408. doi:10.1039/C5CS00113G.

[239] Park G Do, Lee CW, Nam KT. Recent advances and perspectives of halide perovskite photocatalyst. Curr Opin Electrochem 2018;11:98–104. doi:https://doi.org/10.1016/j.coelec.2018.09.009.

[240] Schünemann S, van Gastel M, Tüysüz H, Gastel M, Tüysüz H. A CsPbBr3 /TiO2 Composite for Visible-Light-Driven Photocatalytic Benzyl Alcohol Oxidation. ChemSusChem 2018;11:2057–61. doi:10.1002/cssc.201800679.

[241] Kong Z-C, Liao J-F, Dong Y-J, Xu Y-F, Chen H-Y, Kuang D-B, et al. Core@shell CsPbBr3@zeolitic imidazolate framework nanocomposite for efficient photocatalytic CO2 reduction. ACS Energy Lett 2018;3:2656–62. doi:10.1021/acsenergylett.8b01658.

[242] Hou J, Cao S, Wu Y, Gao Z, Liang F, Sun Y, et al. Inorganic Colloidal Perovskite Quantum Dots for Robust Solar CO2 Reduction. Chem Eur J 2017;23:9481–5. doi:10.1002/chem.201702237.

[243] Xu Y-F, Yang M-Z, Chen B-X, Wang X-D, Chen H-Y, Kuang D-B, et al. A CsPbBr 3 Perovskite Quantum Dot/Graphene Oxide Composite for Photocatalytic CO 2 Reduction. J Am Chem Soc 2017;139:5660–3. doi:10.1021/jacs.7b00489.

[244] Mollick S, Mandal TN, Jana A, Fajal S, Desai A V., Ghosh SK. Ultrastable Luminescent Hybrid Bromide Perovskite@MOF Nanocomposites for the Degradation of Organic Pollutants in Water. ACS Appl Nano Mater 2019:acsanm.8b02214. doi:10.1021/acsanm.8b02214.

[245] Winchester AJ, Petoukhoff C, Abdi-Jalebi M, Andaji-Garmaroudi Z, Pareek V, Wong EL, et al. Investigation of Trap States and Their Dynamics in Hybrid Organic-inorganic Mixed Cation Perovskite Films Using Time Resolved Photoemission Electron Microscopy. 2018 Conf. Lasers Electro-Optics, 2018, p. 1–2.

[246] Li C, Guerrero A, Huettner S, Bisquert J. Unravelling the role of vacancies in lead halide perovskite through electrical switching of photoluminescence. Nat Commun 2018;9:5113. doi:10.1038/s41467-018-07571-6.

[247] Jeangros Q, Duchamp M, Werner J, Kruth M, Dunin-Borkowski RE, Niesen B, et al. In Situ TEM Analysis of Organic–Inorganic Metal-Halide Perovskite Solar Cells under Electrical Bias. Nano Lett 2016;16:7013–8. doi:10.1021/acs.nanolett.6b03158.

[248] Duong T, Mulmudi HK, Shen H, Wu Y, Barugkin C, Mayon YO, et al. Structural engineering using rubidium iodide as a dopant under excess lead iodide conditions for high efficiency and stable perovskites. Nano Energy 2016;30:330–40. doi:https://doi.org/10.1016/j.nanoen.2016.10.027.

[249] Kubicki DJ, Prochowicz D, Hofstetter A, Zakeeruddin SM, Grätzel M, Emsley L. Phase Segregation in Potassium-Doped Lead Halide Perovskites from 39K Solid-State NMR at 21.1 T. J Am Chem Soc 2018;140:7232–8. doi:10.1021/jacs.8b03191.

[250] Kubicki DJ, Prochowicz D, Hofstetter A, Zakeeruddin SM, Grätzel M, Emsley L. Phase Segregation in Cs-, Rb- and K-Doped Mixed-Cation (MA)x(FA)1–xPbI3 Hybrid Perovskites from Solid-State NMR. J Am Chem Soc 2017;139:14173–80. doi:10.1021/jacs.7b07223.

[251] Yong Z-J, Guo S-Q, Ma J-P, Zhang J-Y, Li Z-Y, Chen Y-M, et al. Doping-Enhanced Short-Range Order of Perovskite Nanocrystals for Near-Unity Violet Luminescence Quantum Yield. J Am Chem Soc 2018;140:9942–51. doi:10.1021/jacs.8b04763.

[252] Shai X, Zuo L, Sun P, Liao P, Huang W, Yao E-P, et al. Efficient planar perovskite solar cells using halide Sr-substituted Pb perovskite. Nano Energy 2017;36:213–22. doi:https://doi.org/10.1016/j.nanoen.2017.04.047.

[253] Shahbazi S, Tsai C-M, Narra S, Wang C-Y, Shiu H-S, Afshar S, et al. Ag Doping of Organometal Lead Halide Perovskites: Morphology Modification and p-Type Character. J Phys Chem C 2017;121:3673–9. doi:10.1021/acs.jpcc.6b09722.

[254] Im J, Lee S, Ko T-W, Kim HW, Hyon Y, Chang H. Identifying Pb-free perovskites for solar cells by machine learning. Npj Comput Mater 2019;5:37. doi:10.1038/s41524-019-0177-0.

[255] Xu Q, Li Z, Liu M, Yin W-J. Rationalizing Perovskite Data for Machine Learning and Materials Design. J Phys Chem Lett 2018;9:6948–54. doi:10.1021/acs.jpclett.8b03232.

[256] Liu Y, Li X, Wang J, Xu L, Hu B. An extremely high power factor in Seebeck effects based on a new n-type copper-based organic/inorganic hybrid C6H4NH2CuBr2I film with metal-like conductivity. J Mater Chem A 2017;5:13834–41. doi:10.1039/C7TA03015K.

[257] Xu L, Xiong Y, Mei A, Hu Y, Rong Y, Zhou Y, et al. Efficient Perovskite Photovoltaic-Thermoelectric Hybrid Device. Adv Energy Mater 2018;8:1702937. doi:10.1002/aenm.201702937.

[258] Zhou Y, Yin X, Zhang Q, Wang N, Yamamoto A, Koumoto K, et al. Perovskite solar cell-thermoelectric tandem system with a high efficiency of over 23%. Mater Today Energy 2019;12:363–70. doi:https://doi.org/10.1016/j.mtener.2019.03.003.

[259] He Y, Galli G. Perovskites for Solar Thermoelectric Applications: A First Principle Study of CH3NH3AI3 (A = Pb and Sn). Chem Mater 2014;26:5394–400. doi:10.1021/cm5026766.

[260] Giebink N. Toward Hybrid Organic-Inorganic Perovskite Diode Lasers. Conf. Lasers Electro-Optics, San Jose, California: Optical Society of America; 2018, p. SF1I.1. doi:10.1364/CLEO_SI.2018.SF1I.1.

[261] Ahmad S, George C, Beesley DJ, Baumberg JJ, De Volder M. Photo-Rechargeable Organo-Halide Perovskite Batteries. Nano Lett 2018;18:1856–62. doi:10.1021/acs.nanolett.7b05153.

[262] Giovanni D, Ma H, Chua J, Grätzel M, Ramesh R, Mhaisalkar S, et al. Highly Spin-Polarized Carrier Dynamics and Ultralarge Photoinduced Magnetization in CH3NH3PbI3 Perovskite Thin Films. Nano Lett 2015;15:1553–8. doi:10.1021/nl5039314.

[263] Giovanni D, Chong WK, Dewi HA, Thirumal K, Neogi I, Ramesh R, et al. Tunable room-temperature spin-selective optical Stark effect in solution-processed layered halide perovskites. Sci Adv 2016;2:e1600477. doi:10.1126/sciadv.1600477.

[264] Utzat H, Sun W, Kaplan AEK, Krieg F, Ginterseder M, Spokoyny B, et al. Coherent single-photon emission from colloidal lead halide perovskite quantum dots. Science (80-) 2019;363:1068 LP – 1072. doi:10.1126/science.aau7392.